Singular Value Decomposition and Quasi-Moment-Method as Pathloss Model Calibration Alternatives

H. A. Muhammed[1], A. A. Ayorinde[2], F. O. Okewole[3], M. A. Adelabu[4], A. I. Mowete[5, *]

[1,2,3,4,5] *Department of Electrical and Electronics Engineering, University of Lagos, Akoka, Lagos State, NIGERIA*

Abstract

Using indoor-to-outdoor pathloss measurements for a femtocell network, this paper presents a comparative evaluation of the performances of Singular Value Decomposition (SVD) and Quasi-Moment-Method (QMM) as pathloss model calibration tools. First, the performances of two published SVD models are compared with those of corresponding QMM models, developed through the calibration of basic ECC33 and WINNER II models. Then, and after noting that the 'base models' from which the poorer performing, published SVD calibrations reportedly derive, are either incompletely described or characterized by misprints, alternative 'base models' are prescribed by this paper. It is then shown through analysis that QMM and SVD represent alternative implementations of the same basic model calibration algorithm. Computational results due to the alternative models suggest that better performance metrics (Mean Prediction Error (MPE) and Root Mean Square Prediction Error (RMSPE)) are recorded, when existing basic models are modified to mimic the SVD 'base model', prior to SVD/QMM calibration. Indeed, because the MPE due to the calibration of the alternative models are all close to zero (actually equal to zero in a few cases), the associated residual profiles closely follow the Gaussian distribution typically assumed in the literature, for shadow fading modelling.

Keywords: Singular –value- decomposition, quasi-moment-method, indoor-to-outdoor pathloss, shadow fading

1.0   INTRODUCTION

A number of modelling techniques for the development of empirical models utilized for the prediction of propagation pathloss in indoor, outdoor-to-indoor, and indoor-to-outdoor channels have emerged in recent times. These, for indoor channels, include the 'transport theory' approach described by [1], an approach based on the Kriging algorithm, utilized by [2], and the use by [3], of commercial software to determine pathloss exponent. Many of the outdoor-to-indoor channels modelling approaches generally follow that prescribed by [4], in which 'building penetration' was determined through the calibration of a base model that specified penetration loss as the difference between indoor and outdoor losses. [5], for example, derived an outdoor-to-indoor empirical model by directly modifying the Okamoto-Kitao-Ichitsubo approach through the inclusion of parameters to account for the effects of frequency and building floor height.

*Corresponding author (**Tel:** +234 (0) 8134498678)
Email addresses: hmuhammad@unilag.edu.ng (H. A. Muhammed), aayorinde@unilag.edu.ng (A. A. Ayorinde), fokewole@unilag.edu.ng (F. O. Okewole), amadelabu@unilag.edu.ng (M. A. Adelabu), amowete@unilag.edu.ng (A. I. Mowete)

A related contribution by [6] provided, with a modification of the 3GPP multi-wall model, for attenuation due to internal multi-wall environments, and in addition to penetration loss, investigated the nature of shadow fading associated with predicted pathloss.

[7], based on the outcomes of a dedicated measurement campaign, suggested that the performances of the various multi-wall models should significantly improve if reflection effects are accurately taken into consideration. As implicitly suggested by [7], the multi-wall model is also applicable for modelling of indoor-to-outdoor pathloss; and the outcome of investigations by [8] clearly supp.ort that suggestion.

Two notable modelling techniques for indoor-to-outdoor scenarios are the Trust Region Algorithm (TRA) utilized by [9], and the Singular Value Decomposition (SVD) approach introduced by [10] for the development of pathloss models concerning femtocell networks in residential buildings. This paper's interest is in the SVD approach, with which [10] calibrated two different base pathloss models, to obtain significantly better results than reported by [9]. In particular, the paper first compares the performances of the SVD models presented by [10] with

corresponding models developed with the QMM [11] calibration of basic ECC33 and WINNER II models. The results of the comparisons clearly revealed that across all the four frequencies considered over the four sites treated by [10], the QMM-calibrated models had better MPE and RMSPE metrics than the two SVD models. As examples, in the case of 'Model A' of Allen et al, the best performance was recorded at 0.9GHz, as (MPE, RMSPE) dB = (1.7540, 8.9335) dB, as against (1.1484, 8.3333) dB and (-0.0259, 8.6468) dB for the corresponding QMM-calibrated ECC33 and WINNER II models, respectively. For 'Model B', the best metrics (also at 0.9GHz) were recorded as (-0.0808, 5.0125) dB compared with the respective corresponding metrics of (0.0030, 4.8838) dB and (-0.0284, 4.9722) dB for QMM-calibrated basic ECC33 and WINNER II models. One remarkable outcome of the calibration process is that when the models due to SVD calibration (as reported by [10]) were utilized as base models in QMM-calibration schemes, RMSPE and MPE metrics, significantly better than those of the original models, were recorded.

Although the SVD models defined by the specifications on Tables 2 and 3 of [10] were utilized for the comparisons alluded to in the foregoing discussions, it is evident that the model parameters could not have derived from the 'Design' matrices of the paper's equations (8) and (10), for Models 'A' and 'B', respectively; as both matrices are clearly singular. In order to eliminate the collinearity problem [12] evident in those design matrices, this paper prescribes alternative base models for use with SVD calibration. In addition to yielding significantly improved performance metrics, the computational results obtained from the calibration of the alternative base models verified this paper's analytically established relationship, which demonstrated that basic pathloss model calibration using SVD and QMM represent alternative implementations of the same computational scheme.

The paper in its section 2, presents succinct descriptions of the characteristic features of the SVD and QMM, as utilized for propagation pathloss modelling. Section 3 discusses outcomes of the calibration of some basic pathloss models, and in particular, compares the performances of SVD and QMM as alternative tools. Discussions in the section extend over MPE and RMSPE metrics associated with the calibrated models, as well as shadow fading characteristics owing to the residuals of the prediction models. Important conclusions arising from the analytical and computational results are summarized in section 4, which is the paper's concluding section

2.0   ANALYSIS
Singular Value Decomposition (SVD) and Quasi-Moment-Method (QMM) represent two apparently different additions to the body of knowledge concerning the calibration of basic radiowave propagation pathloss models, in order to predict channel pathloss in various environments. The characterizing features of these modelling tools are briefly described in what follows.

2.1   *Singular Value Decomposition calibration*
As developed by [10] and following an exposition by [12], SVD empirical pathloss models may, in general, be described as deriving from the calibration of basic models of the type defined by

$$P_b(d) = \varphi_1 + \varphi_2 + \ldots + \varphi_N ,\tag{1}$$

for which a set $\{\alpha_n\}_{n=1}^N$ 'of calibration coefficients' can be determined, such that residual function given as

$$\varepsilon = P_{mea}(d) - P_{svd}(d)\tag{2}$$

approximates a zero-mean Gaussian random variable. In Eqn. (2). P_{mea} represents measured pathloss at different points away from the transmitter, whilst $\mathbf{P_{svd}}$ is the outcome of the calibration of P_b, as will be described shortly. It is given by

$$P_{svd} = \alpha_1\varphi_1 + \alpha_2\varphi_2 + \ldots + \alpha_N\varphi_N\tag{3}$$

In order to determine the calibration coefficients of Eqn, (3), the SVD algorithm first defines a 'design matrix' according to

$$[D] = \begin{bmatrix} \varphi_1(d_1) & \varphi_2(d_1) & \cdots & \varphi_N(d_1) \\ \varphi_1(d_2) & \varphi_2(d_2) & \cdots & \varphi_N(d_2) \\ \cdots & \cdots & \cdots & \cdots \\ \varphi_1(d_M) & \varphi_2(d_M) & \cdots & \varphi_N(d_M) \end{bmatrix}\tag{4}$$

an $M \times N$ matrix, whose number of columns (N) is the same as the number of unknown calibration coefficients, and whose number of rows (M) equals the number of points at which pathloss measurements are taken. The desired calibration coefficients (and hence, the SVD model) are then given by [10]

$$\begin{pmatrix} \alpha_1 \\ \alpha_2 \\ \cdots \\ \alpha_N \end{pmatrix} = \left(\begin{bmatrix} \varphi_1 & \varphi_2 & \cdots & \varphi_N \\ \varphi_1 & \varphi_2 & \cdots & \varphi_N \\ \cdots & \cdots & \cdots & \cdots \\ \varphi_1 & \varphi_2 & \cdots & \varphi_N \end{bmatrix}^T \begin{bmatrix} \varphi_1 & \varphi_2 & \cdots & \varphi_N \\ \varphi_1 & \varphi_2 & \cdots & \varphi_N \\ \cdots & \cdots & \cdots & \cdots \\ \varphi_1 & \varphi_2 & \cdots & \varphi_N \end{bmatrix} \right)^{-1} \begin{bmatrix} \varphi_1 & \varphi_2 & \cdots & \varphi_N \\ \varphi_1 & \varphi_2 & \cdots & \varphi_N \\ \cdots & \cdots & \cdots & \cdots \\ \varphi_1 & \varphi_2 & \cdots & \varphi_N \end{bmatrix}^T \begin{pmatrix} P_{mea}(d_1) \\ P_{mea}(d_2) \\ \cdots \\ P_{mea}(d_M) \end{pmatrix}\tag{5}$$

The superscripts on $[\bullet]^T$ and $[\bullet]^{-1}$ appearing in Eqn. (5) denote matrix transposition and inversion, respectively.

2.2   The Quasi-Moment - Method

For the QMM, Eqns. (1) – (3) still apply, but the requirement on Eqn. (2) is that ([11]; [13]) the Euclidean semi-norm of the error function should assume a minimum value; that is

$$\|\varepsilon\|_2 = \|P_{mea} - P_{qmm}\|_2 \qquad (6)$$

should be minimum. Also, in this case, the calibration coefficients are determined through the definition of a 'model calibration matrix' according to [14]

$$[\Phi] = \begin{bmatrix} \langle \varphi_1, \varphi_1 \rangle & \langle \varphi_1, \varphi_2 \rangle & \cdots & \langle \varphi_1, \varphi_N \rangle \\ \langle \varphi_2, \varphi_1 \rangle & \langle \varphi_2, \varphi_2 \rangle & \cdots & \langle \varphi_2, \varphi_N \rangle \\ \cdots & \cdots & \cdots & \cdots \\ \langle \varphi_N, \varphi_1 \rangle & \langle \varphi_N, \varphi_2 \rangle & \cdots & \langle \varphi_N, \varphi_N \rangle \end{bmatrix} \qquad (7)$$

Thereafter, a 'conditioned pathloss vector' is defined as ([11])

$$\left(P_{mea-q}\right) = \begin{pmatrix} \langle \varphi_1, P_{mea} \rangle \\ \langle \varphi_2, P_{mea} \rangle \\ \cdots \\ \langle \varphi_N, P_{mea} \rangle \end{pmatrix} \qquad (8)$$

and the calibration coefficients consequently determined as

$$\begin{pmatrix} \alpha_1 \\ \alpha_2 \\ \cdots \\ \alpha_N \end{pmatrix} = \begin{bmatrix} \langle \varphi_1, \varphi_1 \rangle & \langle \varphi_1, \varphi_2 \rangle & \cdots & \langle \varphi_1, \varphi_N \rangle \\ \langle \varphi_2, \varphi_1 \rangle & \langle \varphi_2, \varphi_2 \rangle & \cdots & \langle \varphi_2, \varphi_N \rangle \\ \cdots & \cdots & \cdots & \cdots \\ \langle \varphi_N, \varphi_1 \rangle & \langle \varphi_N, \varphi_2 \rangle & \cdots & \langle \varphi_N, \varphi_N \rangle \end{bmatrix}^{-1} \begin{pmatrix} \langle \varphi_1, P_{mea} \rangle \\ \langle \varphi_2, P_{mea} \rangle \\ \cdots \\ \langle \varphi_N, P_{mea} \rangle \end{pmatrix} \qquad (9)$$

provided that the inner product quantities appearing in Eqns. (7) – (9) are typified by

$$\langle \varphi_k, \varphi_l \rangle = \sum_{m=1}^{M} \varphi_k(d_m)\varphi_l(d_m) \qquad (10a)$$

and

$$\langle \varphi_k, P_{mea} \rangle = \sum_{m=1}^{M} \varphi_k(d_m)P_{mea}(d_m) \qquad (10b)$$

For the purposes of the comparative evaluation of SVD and QMM as pathloss model calibration tools, four basic models are selected as candidates for calibration, using the indoor-to-outdoor measurement data available, through the use of the commercial software 'GETDATA', from Figures 2(a), 2(b), 3(a) and 3(b) of [10]. The models include those identified as 'Model A' and 'Model B' by [10], for which Eqn. (3), respectively, modifies to

$$P_{svd-A}(d_k) = \alpha_1 * 1 + \alpha_2 * 10\log_{10}(d_k) + \alpha_3 * w \qquad (11)$$

and

$$P_{svd-B}(d_k) = \alpha_1 * 1 + \alpha_2 * 10\log_{10}(d_k) + \alpha_3 * w + \alpha_4 * d_{in} \qquad (12)$$

in both equations, 'w' represents the number of walls located between transmitter and receiver; and the main difference between the two models is the inclusion in 'Model B', of the 'd_in' term, identified as a propagation distance within the indoor environment, separating the transmitter from the wall; and through which net pathloss can be disaggregated into indoor and outdoor components.

The other two candidate base models include the ECC33 model, prescribed as

$$P_{ecc-qmm}(d_k) = \alpha_1 * 92.4 + \alpha_2 * 20\log_{10}(d_k) + \alpha_3 * 20\log_{10}(f) + \alpha_4 * 20.41$$
$$+ \alpha_5 * 9.83\log_{10}(d_k) + \alpha_6 \log_{10}(f)\left[7.894 + 9.56\log_{10}(f)\right]$$
$$+ \alpha_7 * \left[13.98\log_{10}\left(\frac{h_{te}}{200}\right)\right] + \alpha_8 * \left[\log_{10}\left(\frac{h_{te}}{200}\right)\left(-5.8\left(\log_{10}(d_k)\right)^2\right)\right];$$
$$+ \alpha_9 * \left[-42.5\left(\log_{10}(h_{re}) - 0.585\right)\right] + \alpha_{10} * \left[-13.7\log_{10}(f)\left(\log_{10}(h_{re}) - 0.585\right)\right] \qquad (13)$$

In which 'f' represents transmitter operating frequency in (GHz), h_{re}, receiver antenna height, and h_{te}, transmitter antenna height.

And the WINNER II model, which, for line-of-sight scenarios, is defined by

$$P_{WNII-qmm}(d_k) = \alpha_1 * 46.4 + \alpha_2 * 20\log_{10}(d_k) + \alpha_3 * 20\log_{10}\left(\frac{f}{5}\right) \qquad (14)$$

or in the non-line-of-sight case, by

$$P_{WNII-qmm}(d_k) = \alpha_1 * 46.4 + \alpha_2 * 20\log_{10}(d_k) + \alpha_3 * 20\log_{10}\left(\frac{f}{5}\right) + \alpha_4 * 12w \qquad (15)$$

In addition to the QMM-calibration of the base models of Eqns. (13), (14), and (15), the SVD models reported by [10] as deriving from Eqns. (11) and (12) were also subjected to QMM-calibration. Outcomes of the calibrations are presented and evaluated in section 3.

3.0 PERFORMANCE EVALUATION OF QMM AND SVD CALIBRATED MODELS

The models performance evaluation is presented in two broad parts. First, the prediction performances of the SVD models ('A' and 'B') of [10] are compared (essentially in terms MPE and RMSPE) with those of corresponding models developed through QMM calibration, including 're-calibrated Models A and B'. In the second part, the prediction performances of alternative models informed by constraints of the SVD algorithm are compared, also in terms of the conventional performance metrics. For all the computational results concerning the ECC33 models, presented here and elsewhere in the paper, d_k is in meters, with $h_{re} = 1.2m$, and $h_{te} = 1.0m$, as specified by [10].

3.1 Prediction Performances of QMM- and SVD-Calibrated Models

The model calibration coefficients defined by the equations of the preceding sections were obtained through FORTRAN implementations of the algorithms, to define each of the calibrated models, whose predicted pathloss profiles are evaluated in the ensuing discussions.

3.1.1 Calibration with Measurements from Fig (2a) and 2(b) of [10]

The calibration coefficients due to the QMM-calibration of the base models of Eqns. (11), (13), and (14), with measurements available from Figure 2(a) of [10] are summarized in Table 1. It is important to note that the QMM-model coefficients for 'SVD-Model A' in the table represent outcomes of the calibration of the models specified by the Table's fourth column. In the case of 2.5GHz, for example, this implies that

$$P_{qmm-mdlA}(d_k) = 0.1367(44.7*1) + 0.8403(3.48*10\log_{10}(d_k)) + 4.7982(11.3*w) \quad (16)$$

in which the numerical values in magenta coloured font are the coefficients due to QMM calibration using the 2.5GHz pathloss measurements of Figure 2(a) of [10], with w = 1 in all cases.

Table 1: Model calibration coefficients for calibration with measurements of Figure 2(a) of [10]

Frequency (GHz)	QMM Models ECC33 $(\alpha_1, \alpha_2, \ldots \alpha_{10})$			WINNERII $(\alpha_1, \alpha_2, \alpha_3)$			SVD-MODELA $(\alpha_1, \alpha_2, \alpha_3)$			SVD-Model A Allen et al $(\alpha_1, \alpha_2, \alpha_3)$
0.9	0.9048 -5.9450 27.0124 -5.2545 9.9616 16.3448 1.3524 1.2431 -0.3191- 320.64767			-0.5352	1.5672	- 5.0111	0.5795	0.9017	4.2117	35.65, 3.25, 6.87
2.0	0.1513 -8.0733 10.0862 2.5045 15.5707 -1.1753 -1.3350 0.9745 0.0523 - 0.4243			0.6572	1.4319	-3.9651	-0.4702	0.7784 9.2676		39.54, 3.44, 8.73
2.5	0.0169 0.5065 6.5004 1.7475 -0.9103 0.5617 - 2.6733 0.7270 0.2628 24.1764			0.6419	1.5637	-5.0307	0.1367	0.8403	4.7982	44,70, 3.48, 11.30
3.5	0.6050 4.1995 4.9230 0.9806 -6.4713 6.0553 0.3848 0.2421 -0.7980 - 25.6654			0.3389	1.5458	- 16.0743	0.8551	0.7834	2.0769	48.73,3.69, 11.55

Profiles of the pathloss predicted by the models on Table 1 are displayed in Figure (1), from which, it can be seen that although the 'Model-A' profiles for 0.9GHz and 2.0GHz compare favourably with the corresponding QMM models, those for 2.5GHz and 3.5GHz do not. The MPE and RMSPE metrics for the models are available from Table 2, and the metrics confirm the foregoing observation. As the metrics in Table 2 reveal, the re-calibration of 'Model-A' attracted virtually 100% improvements in MPE at all the frequencies.

On the other hand, associated improvements in RMSPE ranged from about 3% at 0.9GHz through 7.3% (2.0GHz) and 13.4% (2.5GHz) to 26.9% at 3.5GHz.
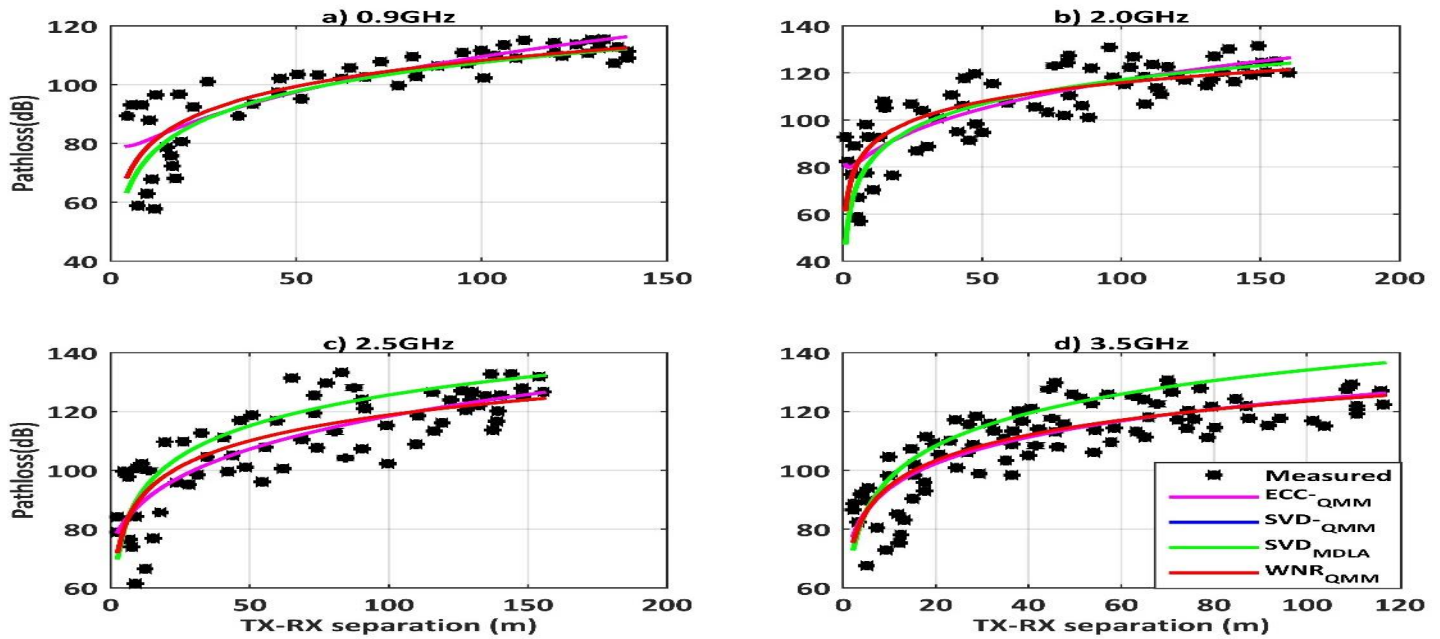
Figure 1: Pathloss profiles predicted by models SVD and QMM calibrated with measurements of Figure 2(a) of [10]

Table 2: Mean Prediction and Root Mean Square Prediction Errors due to the models defined by Table 1

FREQ /	0.9GHz		2.0GHz		2.5GHz		3.5GHz	
MODEL	MPE	RMSPE	MPE	RMSPE	MPE	RMSPE	MPE	RMSPE
$A_{[10]}$	1.7540	8.9335	1.3865	11.4181	-5.0713	11.4258	-6.9140	11.2200
A_{QMM}	0.0008	8.6466	-0.0012	10.5799	-0.0025	9.8993	0.0003	8.2016
ECC_{QMM}	-0.2475	8.2562	1.8733	9.9392	0.0234	9.6577	-0.4706	8.1885
WIN_{QMM}	-0.0259	8.6468	-0.0004	10.5799	0.0010	9.8993	-0.0003	8.2016
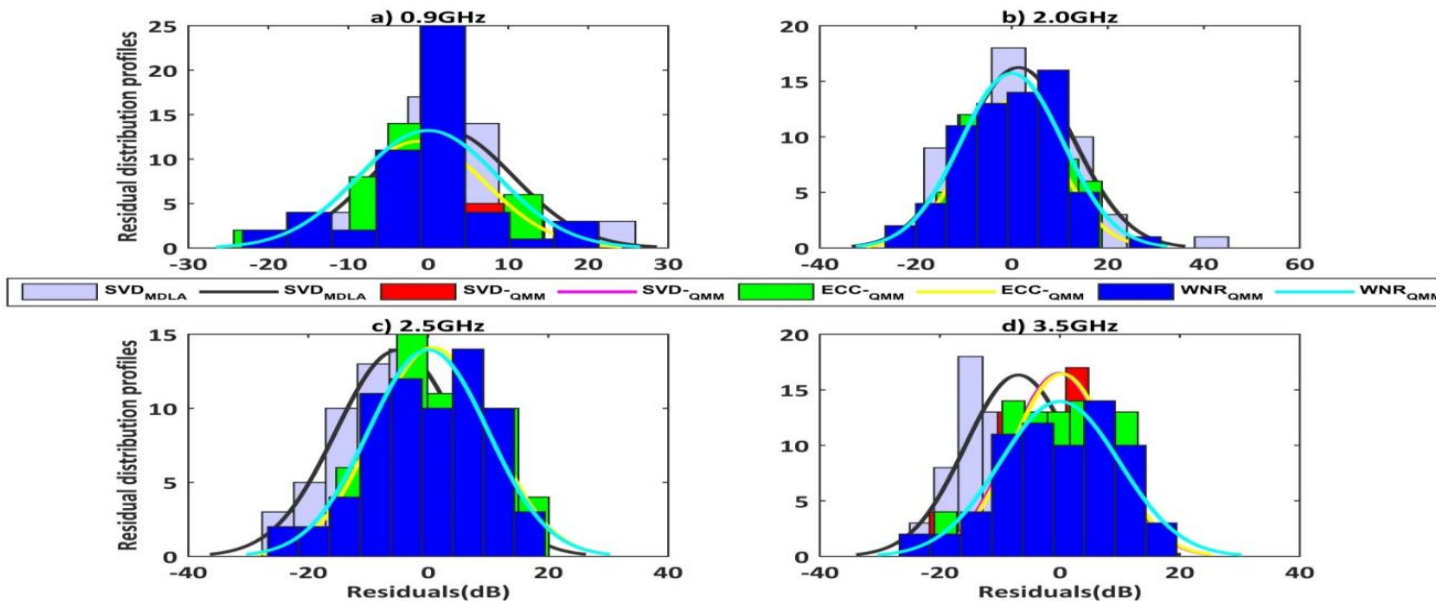
Figure 2: Histograms and normal density functions for residuals of the calibrated models of Table 1.

It is also to be observed that whereas the QMM 'Model A' and 'WINNER II' models have identical RMSPE metrics across frequencies considered, corresponding MPE values differ, with the latter being slightly better on the net. One interesting outcome of the calibrations is that the calibrated ECC33 models recorded

the best RMSPE metrics, though at the expense of MPE performance.

It is customary in indoor-to-outdoor empirical pathloss investigations [9], [10], [15] to model 'shadow fading' as being manifested by the random variation of the residuals of the calibrated model about the mean and variance. For the models defined by coefficients on Table 1, statistical descriptions of the residuals are provided by histogram and normal probability plots of Figures (2) and (3). The profiles reveal that the distributions of the residuals for the models are all approximately Gaussian as expected, though unlike the profiles for the QMM-models, those for

the SVD models have significant departures from zero-mean, particularly at 2.5GHz and 3.5GHz.

And this observation is supported by the normal probability curves of Figure (3), in which most of the profiles approximate the straight line characteristic of the ideal Gaussian distribution, with the 'S-shaped' curve for the SVD model at 900MHz suggesting that the distribution of the residuals is in this case, bimodal. It is also to be observed that despite the differences in the profiles, they all predict about the same levels of extreme interference, as indicated by the boundary values of variations about the mean.
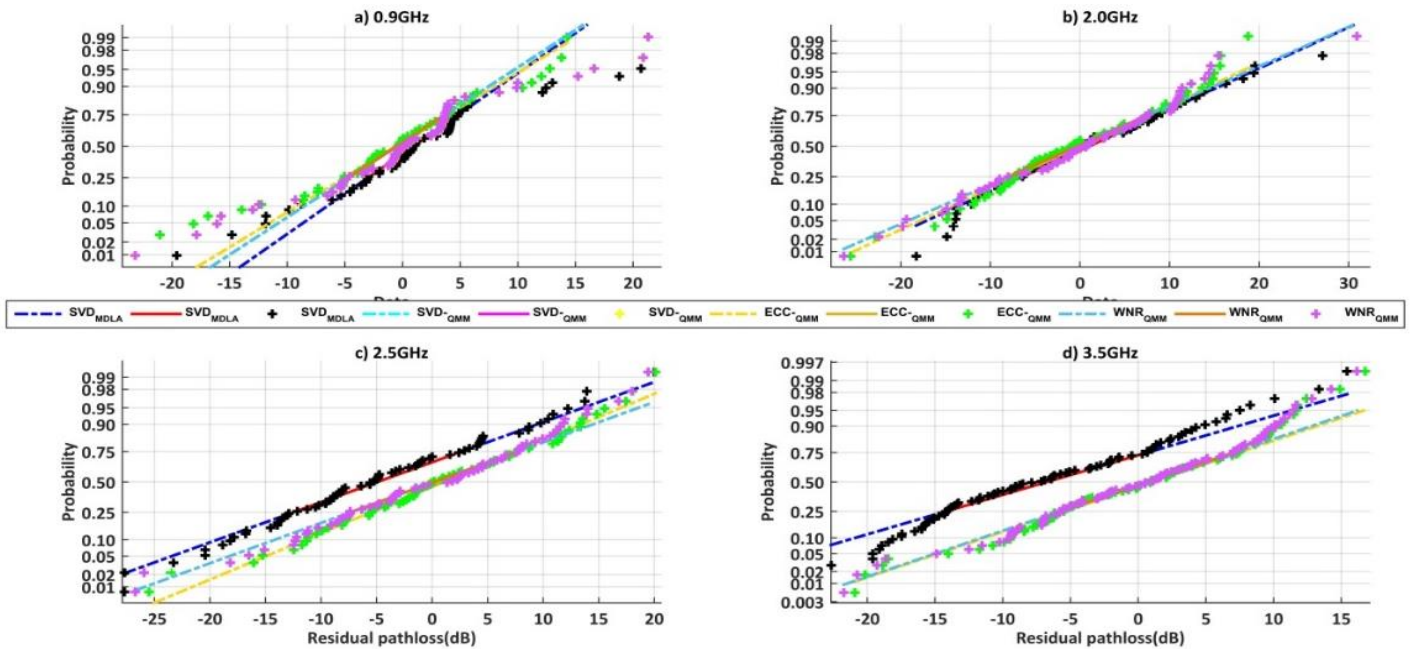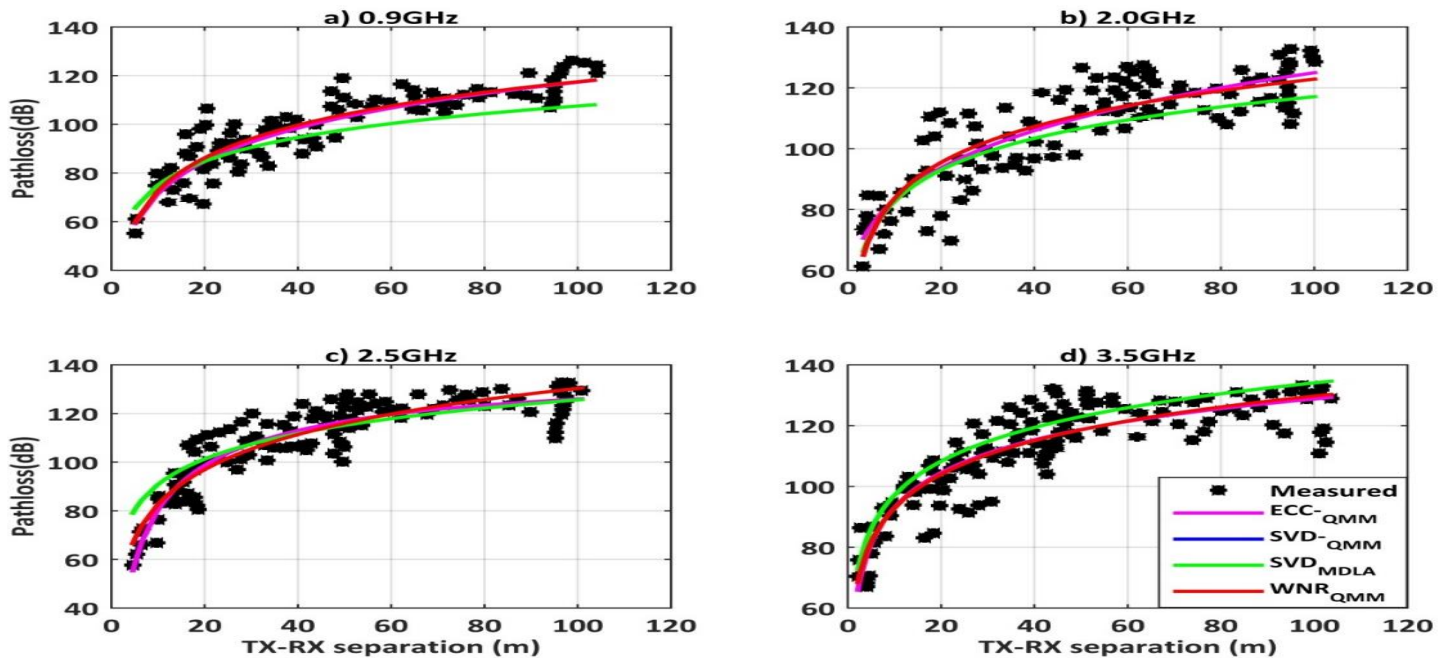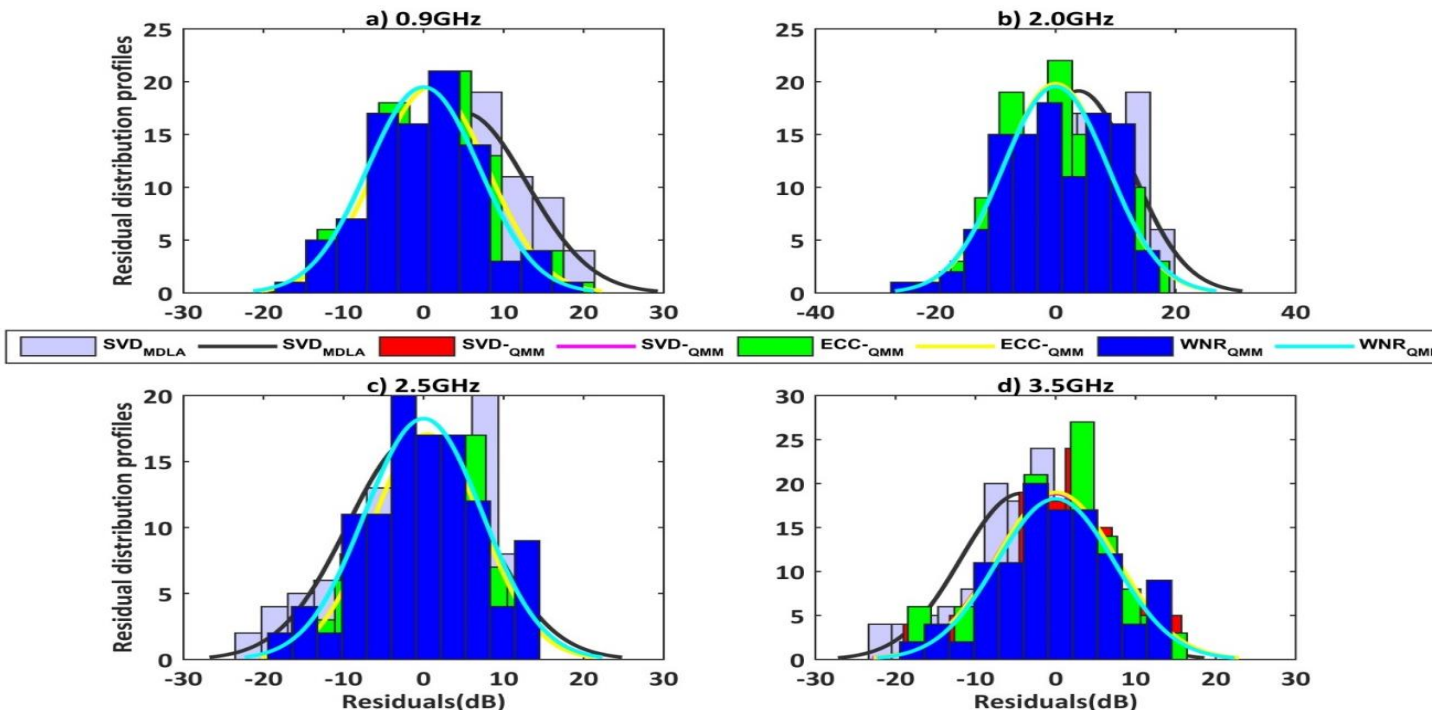

Figure 3: Normal probability plots for the profiles of Figure (2)

Table 3: Model calibration coefficients from calibration with measurements of Figure 2(b) of [10]

Frequency(GHz)	QMM Models ECC33 $(\alpha_1, \alpha_2, \ldots \alpha_{10})$	WINNERII $(\alpha_1, \alpha_2, \alpha_3)$	SVD-MODEL A $(\alpha_1, \alpha_2, \alpha_3)$	SVD-Model A Allen et al $(\alpha_1, \alpha_2, \alpha_3)$
0.9	-0.0602 -1.0294 -11.0155 -0.4047 5.6079 -69.9150 0.3491 0.2576-1.7454 -131.2284	0.0999 2.3987 -1.5525	0.5795 0.9017 -4.2117	35.65, 3.25, 6.87
2.0	0.7046 -2.2125 -2.7050 1.2469 5.6672 -0.4446 -0.3915 0.7527 2.1352 -21.5199	0.6052 2.0958 -2.0275	0.3069 1.1393 3.7028	39.54, 3.44, 8.73
2.5	0.1720 0.4918 -3.6791 0.0718 10.2923 -1.3258 -0.4696 -1.6362 0.8088 2.6633	-2.0927 2.5508 -22.0687	0.3521 1.3707 1.6983	44,70, 3.48, 11.30
3.5	0.1893 2.3348 0.7704 -1.2165 -0.1683 0.7853 1.7934 -0.2350 -1.3584 4.2853	0.2370 1.9675 -14.5398	1.2564 0.9971 -0.4404	48.73,3.69, 11.55

Table 4: Mean Prediction and Root Mean Square Prediction Errors due to the models of Table 3

FREQ / MODEL	0.9GHz		2.0GHz		2.5GHz		3.5GHz	
	MPE	RMSPE	MPE	RMSPE	MPE	RMSPE	MPE	RMSPE
$A_{[10]}$	4.8957	9.3577	3.8264	9.7074	-0.9809	8.5108	-4.3084	8.6494
A_{QMM}	-0.0023	6.9557	0.0008	8.7464	0.0008	7.3116	-0.0027	7.4999
ECC_{QMM}	-0.1993	6.9475	0.4758	8.6077	0.1019	6.8132	0.0643	7.4764
WIN_{QMM}	-0.0009	6.96	0.0020	8.7464	0.0027	7.3116	-0.0003	7.4999

Figure 4: Pathloss profiles predicted by models SVD and QMM calibrated with measurements of Figure 2(b) of [10]

Figure 5: Histograms and normal density functions for residuals of the calibrated models of Table 3
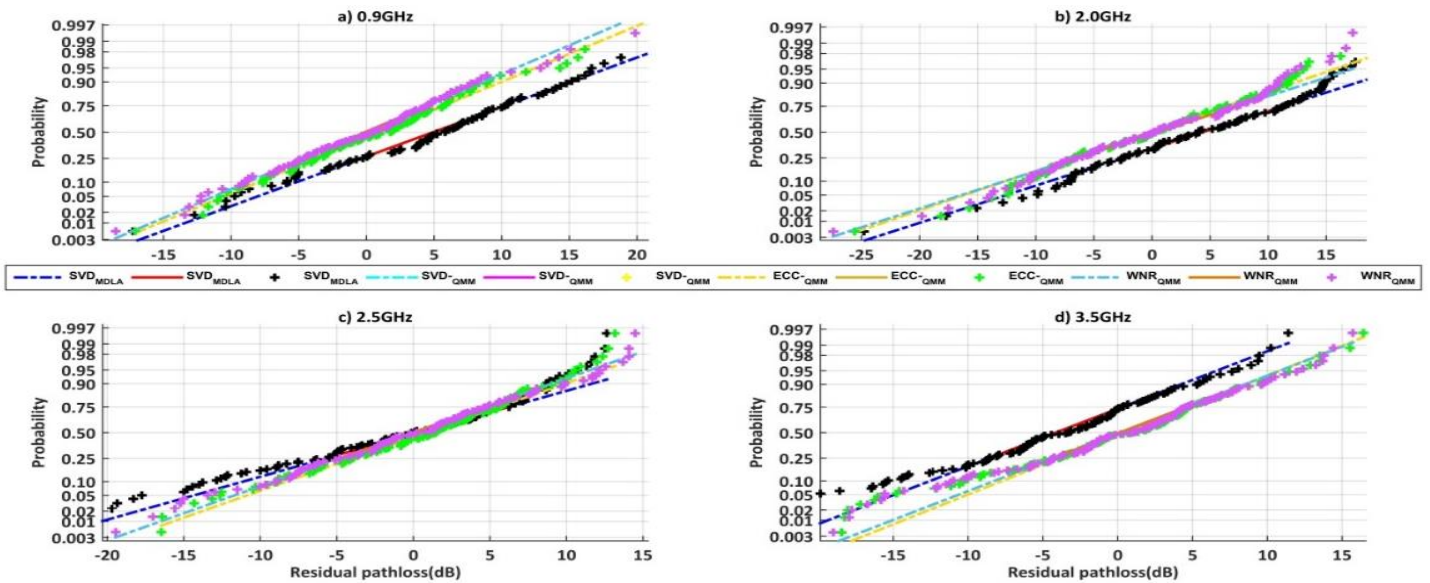
Figure 6: Normal probability plots for the profiles of Figure (5)

Table 5: Model calibration coefficients from calibration with measurements of Figure 3(a) of [10]

Frequency (GHz)	QMM Models			SVD-Model B
	ECC33 $(\alpha_1, \alpha_2, \ldots \alpha_{10})$	WINNERII $(\alpha_1, \alpha_2, \alpha_3, \alpha_4)$	SVD-MODELB $(\alpha_1, \alpha_2, \alpha_3, \alpha_4)$	Allen et al $(\alpha_1, \alpha_2, \alpha_3, \alpha_4)$
0.9	0.0278 -1.2044 -14.0882 0.8681 4.1516 53.6005 -1.1861 0.3792 2.5173 -96.4124	4.8064 1.5244 3.4902 17.0716 -31.0334	-6.4634 0.9498 23.4609 7.6253	34.93, 3.21, 5.01, 1.15
2.0	-0.4287 4.9754 10.4961 -8.6442 - 9.8742 -12.4306 3.7620 0.6275 11.0978 -39.3863	-2.4787 1.2668 -12.3361 6.2368 -3.6695	-1.8348 0.7451 - 40.1219 85.1546	38.86, 3.40, 6.85, 1.72
2.5	2.4968 -8.8702 -56.6661 38.9732 18.0818 -17.7205 31.6456 0.8542 - 79.1345 99.8579	0.8535 1.5657 -3.2187 1.8717 -2.4254	8.1059 0.9100 -5.9380 -25.8978	43.78, 3.44, 5.86, 1.72
3.5	0.5156 2.7466 1.3363 -1.3239 - 4.9873 -4.2018 -0.8174 0.6914 1.3141 20.4394	-3.4133 1.5405 -78.0883 -5.0730 6.2969	0.9273 0.6581 9.1969 -11.3936	46.64, 4.68, 11.21, 3.17

A further evaluation of the 'SVD Model A' is provided by the calibration of the base models, using the pathloss measurements available from Figure 2(b) of [10]. Model calibration coefficients obtained in this case are displayed in Table 3. Corresponding mean prediction and Root Mean Square Prediction errors due to these models are presented in Table 4, whose entries generally follow the patterns earlier described for metrics in Table 2. In this case, RMSPE metrics for the QMM-recalibrated 'Model A' improved over those due to [10] by 25% at 0.9GHz, 10%, at 2.0GHz, 14% at 2.5GHz, and 13% at 3.5GHz. Profiles of pathloss predicted by the models are shown in Figure 4.

Figures (5) and (6) describe respectively the histogram / density function and normal probability characteristics of the residuals of the models. The key differences between the sets of curves of Figures (2) and (3)

on one hand, and (5) and (6) on the other are typified by breaks in the neighbourhood of the middle of the graphs for the 'SVD Model A', which are indicative of abnormalities in distribution of the models' residuals.

3.1.2   Calibration with Measurements from Fig (3a) and (3b) of [10]

Calibration coefficients obtained from QMM calibrations with measurements available from Fig, 3(a) of [10] are displayed in Table 5. The objective in this case, is to compare the performances of the SVD 'Models B '([10], Table 3) with those of corresponding QMM models.

The same basic ECC33 model as in the previous cases was calibrated, but in the cases of the WINNERII and SVD-Model B base models, Eqns. (12) (with d_{in} = 5, and w =2) and (15) (with w = 2) were utilized, respectively. Table

6 displays the MPE and RMSPE metrics for the models, and it can be seen from the table that with the exceptions of the models for 2.5GHz and 3.5GHz, the metrics for the SVD models compare favourably with those for the re-calibrated versions. RMSPE improvements due to recalibration emerged as 0.8% at 900MHz and about 7% at 2GHz; as against 16% at 2.5GHz and close to 60% at 3.5GHz. These metrics are reflected by the predicted pathloss profiles of Figure 7, as well as Figures (8) and (9) for the histogram and normal probability plots, respectively.

Table 6: MPE and RMSPE metrics due to models defined by Table 5

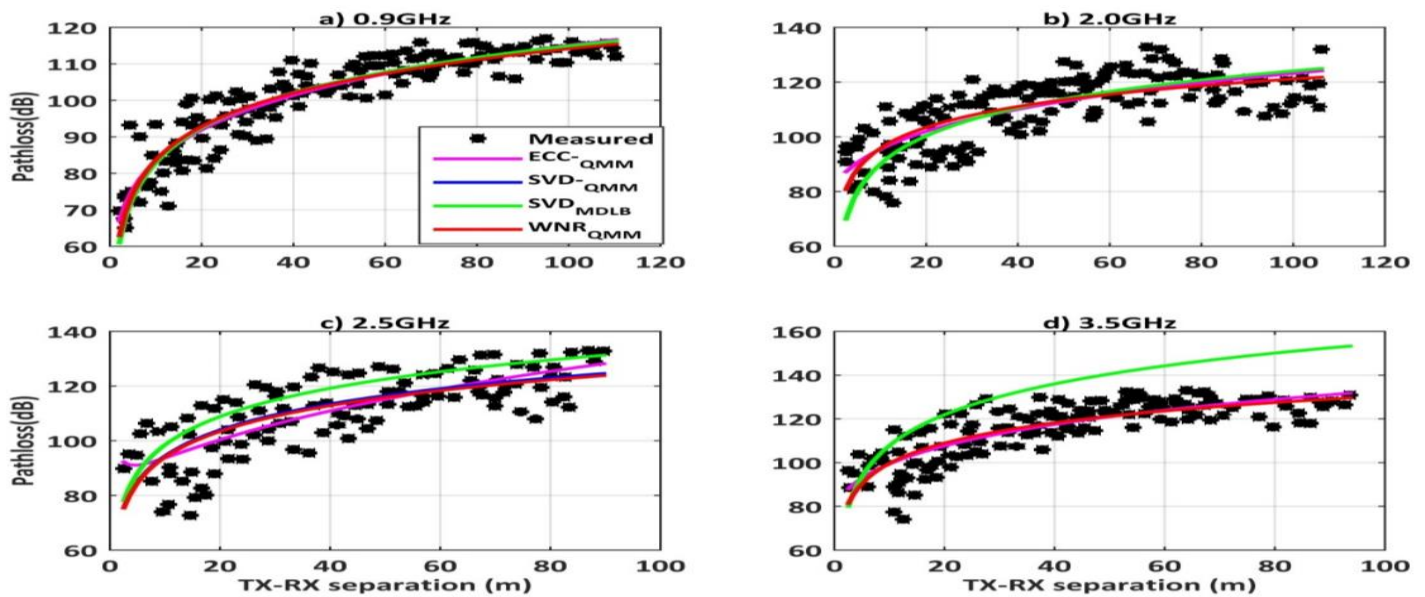| FREQ / MODEL	0.9GHz		2.0GHz		2.5GHz		3.5GHz	
	MPE	RMSPE	MPE	RMSPE	MPE	RMSPE	MPE	RMSPE
$B_{[10]}$	-0.0808	5.0125	0.8202	8.9665	-6.1706	11.4330	-16.5633	19.1123
B_{QMM}	-0.0038	4.9722	-0.0151	8.3516	-0.6151	9.5891	0.0017	7.8240
ECC_{QMM}	0.0035	4.8830	-0.0033	8.2216	-0.0078	9.2030	--0.0006	7.6927
WIN_{QMM}	-0.0009	4.9722	-0.0027	8.3516	-0.0006	9.5685	0.0075	7.8240

Figure 7: Pathloss profiles predicted by models SVD and QMM calibrated with measurements of Figure 3(a) of [10]
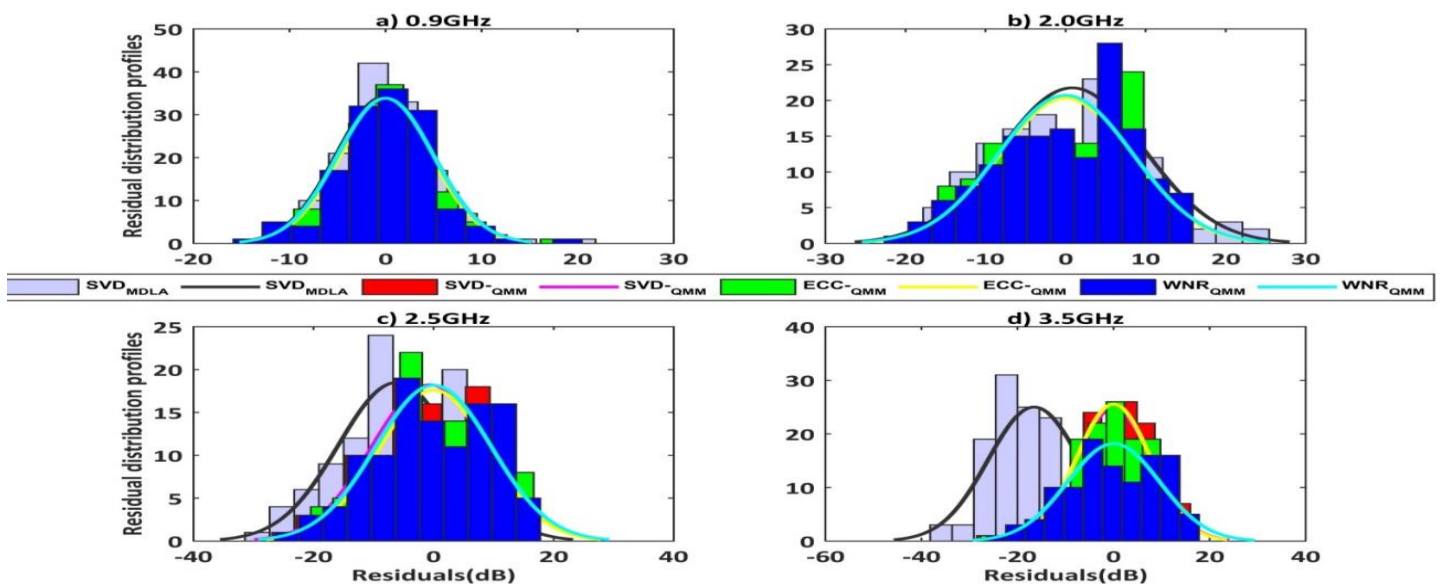

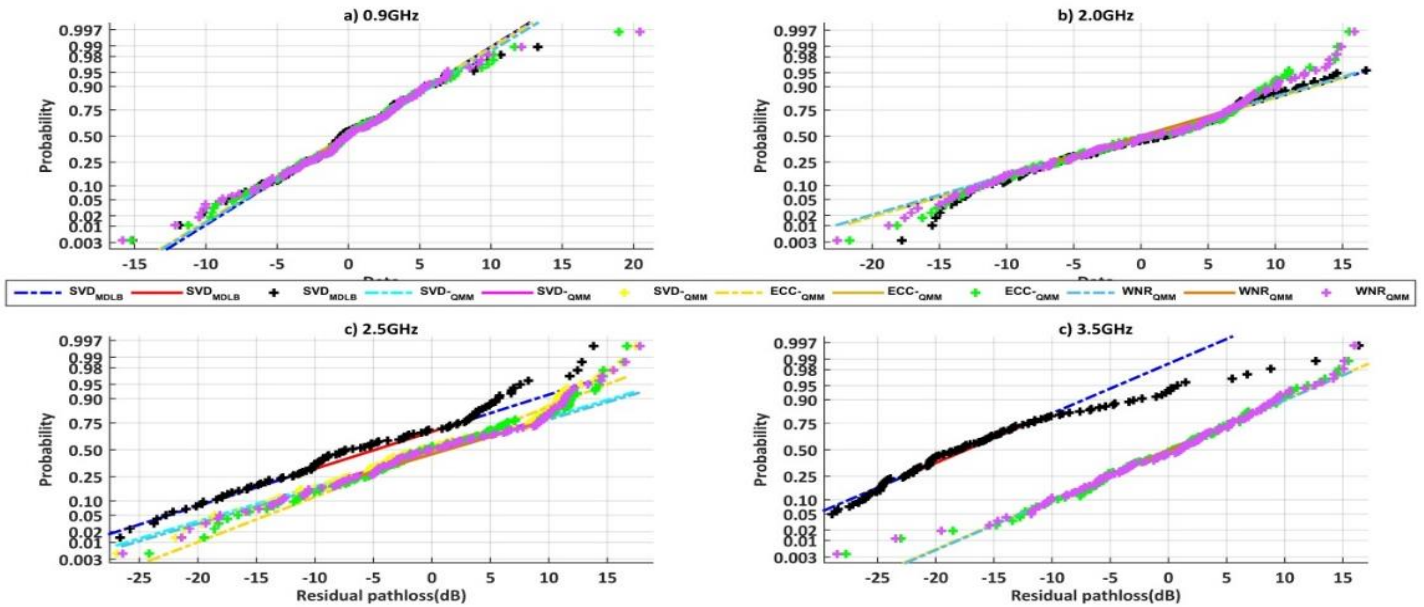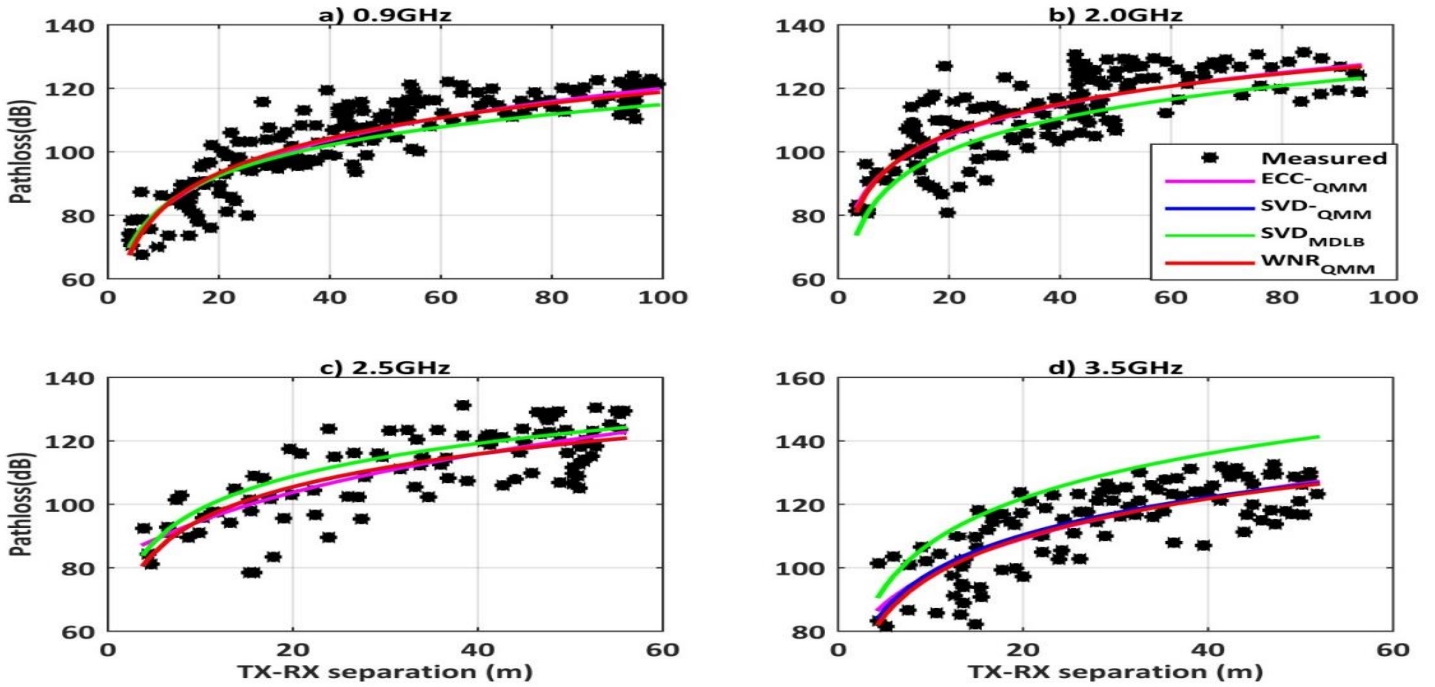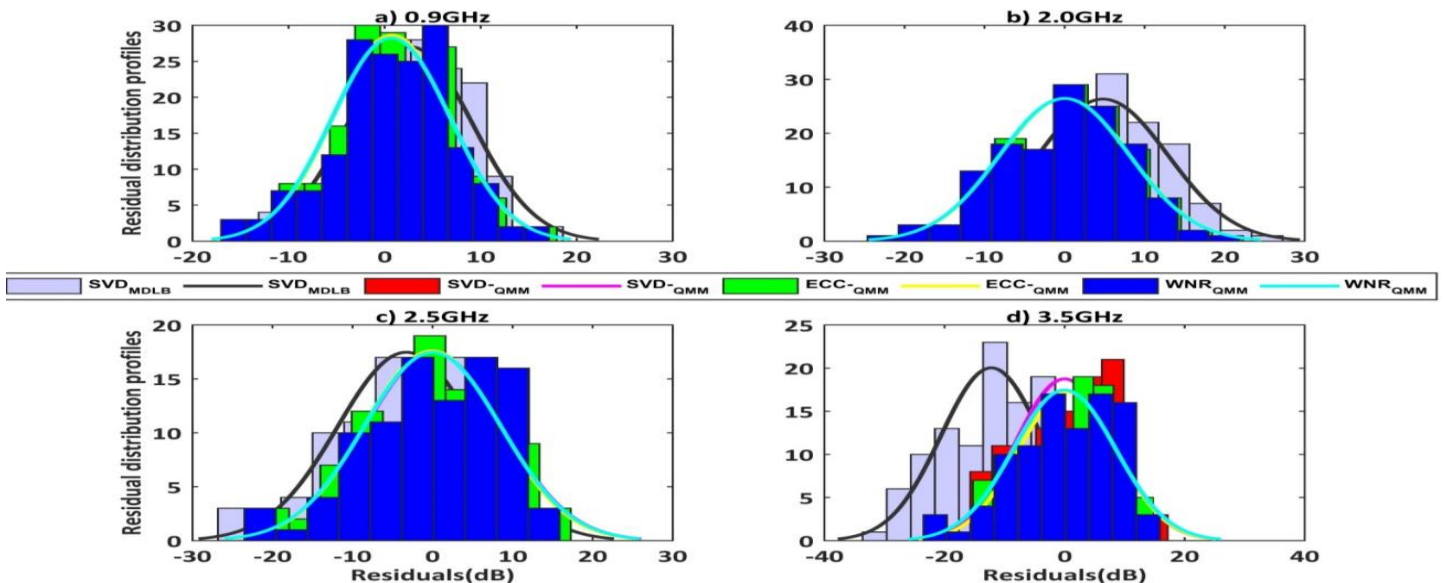**Figure 8:** Histograms and normal density functions for residuals of the calibrated models of Table 5

Figure 9: Normal probability plots for the profiles of Figure (8)

Table 7: Model calibration coefficients from calibration with measurements of Figure 3(b) of [10]

Frequency(GHz)	QMM Models			SVD-Model B
	ECC33 $(\alpha_1, \alpha_2, \ldots \alpha_{10})$	WINNERII $(\alpha_1, \alpha_2, \alpha_3, \alpha_4)$	SVD-MODEL B $(\alpha_1, \alpha_2, \alpha_3, \alpha_4)$	Allen et al $(\alpha_1, \alpha_2, \alpha_3)$
0.9	-0.0451 2.4298 -46.3033 1.8298 -2.8288 41.7228 -0.0201 0.4191 0.4497 45.0233	0.9187 1.8249 15.2549 -3.1227 17.9600	-2.3446 1.1370 6.6823 10.5652	34.93, 3.21, 5.01, 1.15
2.0	-0.0746 -1.2589 18.3012 5.5957 4.9752 7.7370 -7.6173 0.2119 8.8662 -56.9649	-0.9285 1.5727 -7.4285 1.9009 0.1796	[5.5598 0.9251 22.7734 -58.9901	38.86, 3.40, 6.85, 1.72
2.5	3.8553 7.7004 19.3725 -7.9689 -16.6393 -31.0816 18.0011 1.2847 -7.8856 -190.4838	-2.9250 1.7223 3.2484 -0.9549 14.0538	3.0771 1.0015 0.8029 -9.7078	43.78, 3.44, 5.86, 1.72
3.5	-0.4437 1.7972 -0.5691 0.9131 -2.0138 7.0787 0.6545 0.6821 0.5657 4.8162	0.1291 2.0430 8.2730 0.8794 3.2236	0.9273 0.6581 9.1969 -11.3936	46.64, 4.68, 11.21, 3.17

As a matter of fact, Figs 8(d) and 9(d) underscore the notable departure of the SVD-Model B profiles from all the QMM profiles, evidently on account of the very large values of MPE and RMSPE.

Outcomes of the calibration of the same models with measurements available from Fig 3(b) of [10] are identified by the calibration coefficients of Table 7.

MPE and RMSPE metrics recorded for the models defined by Table 7 are shown in Table 8, from which it is evident that the relationship between them generally follows that described for Table 6 in that the most

pronounced difference between the SVD model and its recalibrated version occurred at 2.5GHz, for which a 45% RMSE improvement was recorded by the recalibrated version over the 'SVD Model B'. Corresponding values for the other frequencies are 11.5% (0.9GHz), 14.4% (2GHz), and 6.12% for 2.5GHz.

Profiles displayed in Figure (10) compare pathloss predicted by the models with the corresponding measurement from which they derive, whilst the histogram and normal probability plots of Figs (11) and (12) indicate that the residuals of models describe their shadow fading

properties, reflecting the fact (particularly for the 2.0GHz and 2.5GHz plots) that unlike those for the QMM models, the SVD Model B residuals vary randomly about a mean significantly displaced from zero.

Table 8: Mean Prediction and Root Mean Square Prediction Errors due to the models of Table 7

FREQ / MODEL	0.9GHz		2.0GHz		2.5GHz		3.5GHz	
	MPE	RMSPE	MPE	RMSPE	MPE	RMSPE	MPE	RMSPE
$B_{[10]}$	2.6643	6.9751	4.7946	9.3915	-3.2867	9.1192	-12.2181	14.7963
B_{QMM}	0.6946	6.1720	0.0049	8.0349	0.0959	8.5069	0.0001	8.1295
ECC_{QMM}	0.6786	6.0855	0.0212	8.0264	-0.0187	8.3663	-0.0370	8.0964
WIN_{QMM}	0.6972	6.1723	0.0015	8.0349	-0.0067	8.5064	0.8101	8.1776

Figure 10: Pathloss profiles predicted by models SVD and QMM calibrated with measurements of Figure 3(b) of [10]

Figure 11: Histograms and normal density functions for residuals of the calibrated models of Table 7
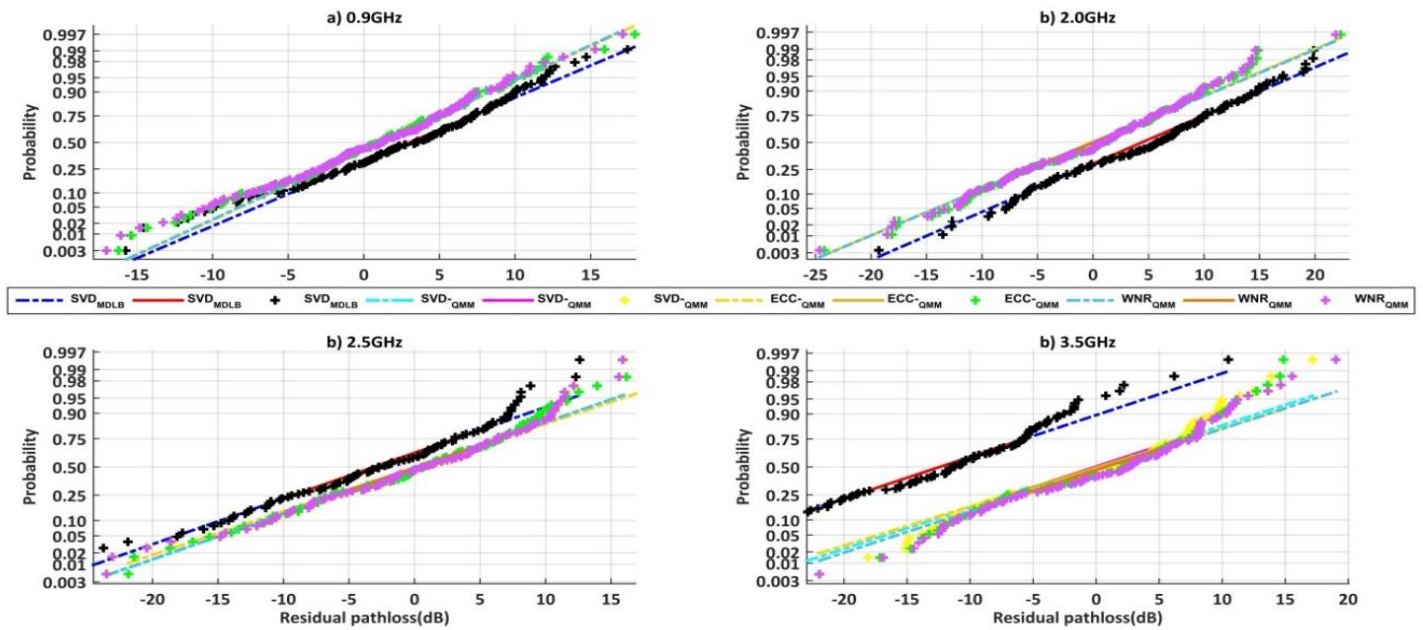
Figure 12: Normal probability plots for the profiles of Figure (11)

3.2   Alternative base models

Because the SVD 'design matrices' specified by Eqns. (8) and (10) of [10] (with 'w' = 1 and 2, respectively) clearly lead to singular $[D]^T[D]$ matrices, as is readily verified, it follows that the 'calibration coefficients' of the publication's Tables 2 and 3 could not have derived from those design matrices; with the further implication that the comparisons of the QMM and SVD algorithms presented in this paper's previous section may not correctly reflect the relationship between them. As a matter of fact, with [D] specified in the form of Eqn. (4), it is easy to show that

$$[D]^T[D] = [\Phi],\tag{17}$$

and that

$$[D]^T(P_{mea}) = (P_{mea-q})\tag{18}$$

in which (P_{mea-q}) and $[\Phi]$ are given by Eqn. (8) and (9), respectively. According to Eqn. (17) and (18) therefore SVD and QMM pathloss calibration algorithms are not two different approaches, but equivalent alternative implementations of the same algorithm.

It is consequently the main objective of this section, to investigate the nature of the equivalence of SVD and QMM as alternative pathloss model calibration tools. And to that end, alternative base models, which eliminate the singularities of the design matrices of [10], while retaining their basic structure are prescribed as follows:

$$[D]_{MDX} = \begin{bmatrix} 1.002+0.003(1-1) & 10\log_{10}(d_1) & 1 \\ 1.002+0.003(2-1) & 10\log_{10}(d_2) & 1 \\ \cdots & \cdots & \cdots \\ 1.002+0.003(M-1) & 10\log_{10}(d_M) & 1 \end{bmatrix}\tag{19}$$

in place of Eqn. (8) of [10], and

$$[D]_{MDY} = \begin{bmatrix} 1.002+0.003(1-1) & 10\log_{10}(d_1) & 2 & d_1/d_{in} \\ 1.002+0.003(2-1) & 10\log_{10}(d_2) & 2 & d_2/d_{in} \\ \cdots & \cdots & \cdots & \cdots \\ 1.002+0.003(M-1) & 10\log_{10}(d_M) & 2 & d_M/d_{in} \end{bmatrix}\tag{20}$$

for 'Model B' of [10]. The ECC33 and WINNERII models are also rearranged to have similar structures according to the set of five (5) 'basis' functions given as:

$$\{\varphi_{ECC}\} = \begin{cases} 1.002+0.003(k-1), & (92.4+20\log_{10}d_k+20\log_{10}f), \\ (20.4+9.83\log_{10}d_k+\log_{10}f(7.894+9.56\log_{10}f)), \\ (-13.98\log_{10}(h_{te}/200)+\log_{10}(h_{te}/200)(-5.8(\log_{10}d_k)^2+(-42.57(\log_{10}h_{re}-0.585)), \\ (-13.7\log_{10}f(\log_{10}h_{re}-0.585)) \end{cases}\tag{21}$$

for the base ECC33 model; and in the case of the base WINNERII (line-of-sight) model, the three 'basis functions' of Eqn. (22a).

$$\{\varphi_{WNI-LI}\} = \{1.002 + 0.003(k-1), \ (46.4 + 18.7\log_{10}d_k), (20\log_{10}(f/5.0))\} \quad (22a)$$

The corresponding Non-Line-of-Sight model is defined by

$$\{\varphi_{WNI-NLI}\} = \{1.002 + 0.003(k-1), \ (46.4 + 20\log_{10}d_k, (20\log_{10}(f/5.0), 24\} \quad (22b)$$

3.2.1 Calibration with measurements of figure 2(a) and 2(b) of [10]

The model calibration coefficients obtained from the calibrations of the alternative models of Eqn. (19), (21) and (22) with measurements available from Figure 2(a) of [10] are displayed in Table 9. It is immediately apparent from these coefficients that SVD and QMM represent alternative implementations of the same pathloss model calibration algorithms. This is very clearly demonstrated by the MPE and RMSPE metrics recorded by these alternative models as shown in Table 10.

Table 9: Calibration coefficients for the alternative models

Frequency (GHz)	QMM Models ECC33 $(\alpha_1, \alpha_2, \ldots \alpha_5)$	WINNERII $(\alpha_1, \alpha_2, \alpha_3)$	MODEL X $(\alpha_1, \alpha_2, \alpha_3)$	SVD MODEL X $(\alpha_1, \alpha_2, \alpha_3)$
0.9	-234.1387 3.8215 -12.2547 2.3782 -311.3050-	72.6695 1.1852 4.8256	72.7021 2.2158 - 16.9129	72.8140 2.2148 - 17.0155
2.0	-165.6378 5.8801 -14.0668 1.7901 -43.8989	119.3398 0.8075 10.9289	119.3895 1.5095 - 49.5588	119.3548 1.5098 - 49.5265
2.5	-111.2610 -1.2578 1.1821 1.4440 77.9728	72.4753 1.1112 9.4379	72.5308 2.0773 - 5.3146	72.4130 2.0787 - 5.2080
3.5	-276.4738 -0.0321 -2.0664 2.7967 72.0655	12.7499 1.4239 3.6739	12.7298 2.6631 54.7037	12.6498 2.6645 54.7727

Table 10: MPE and RMSPE for the calibrated alternative models

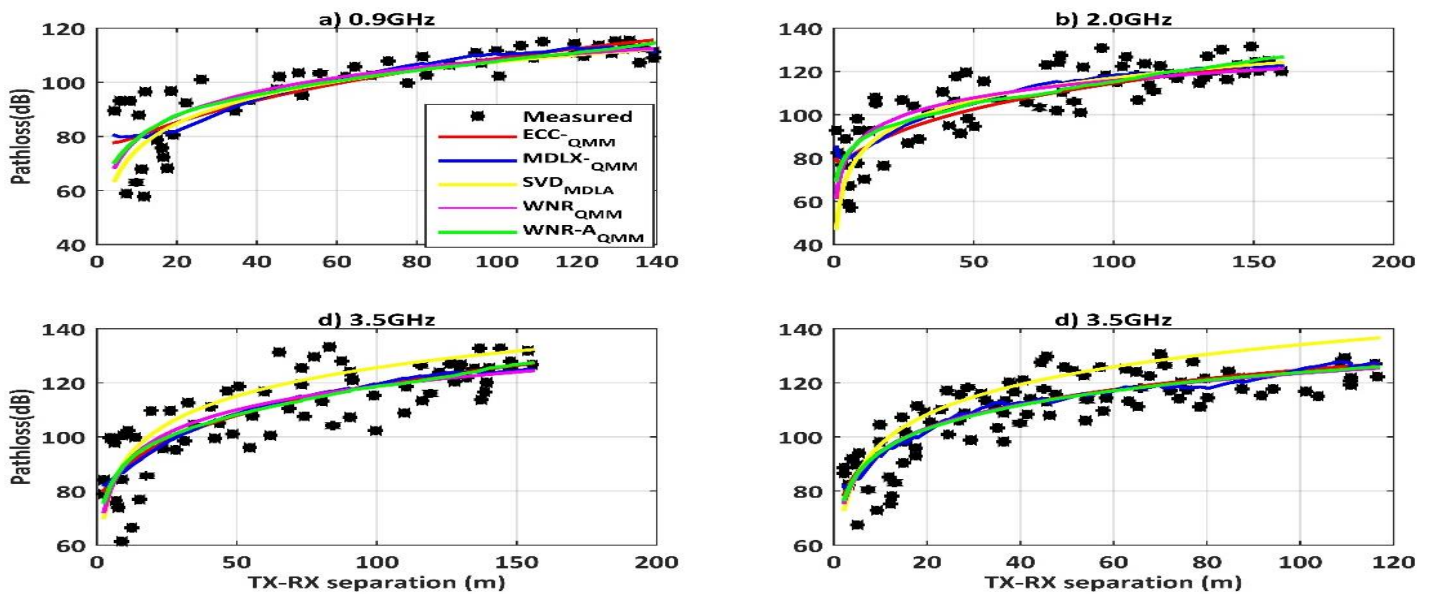| FREQ / MODEL	0.9GHz		2.0GHz		2.5GHz		3.5GHz	
	MPE	RMSPE	MPE	RMSPE	MPE	RMSPE	MPE	RMSPE
X_{SVD}	-0.0006	8.5966	0.0001	10.2055	0.0003	9.7787	0.0003	8.1951
X_{QMM}	0.0008	8.5966	-0.0008	10.2056	0.0003	9.7787	0.0000	8.1951
ECC_{QMM}	-0.1175	8.0489	-0.1318	9.5874	0.0074	9.6036	-0.0169	8.0352
WIN_{QMM}	-0.0038	8.5966	-0.0007	10.2055	-0.0015	9.7787	-0.0027	8.1951

Figure 13: Comparison of pathloss predicted by calibrated base and alternative models
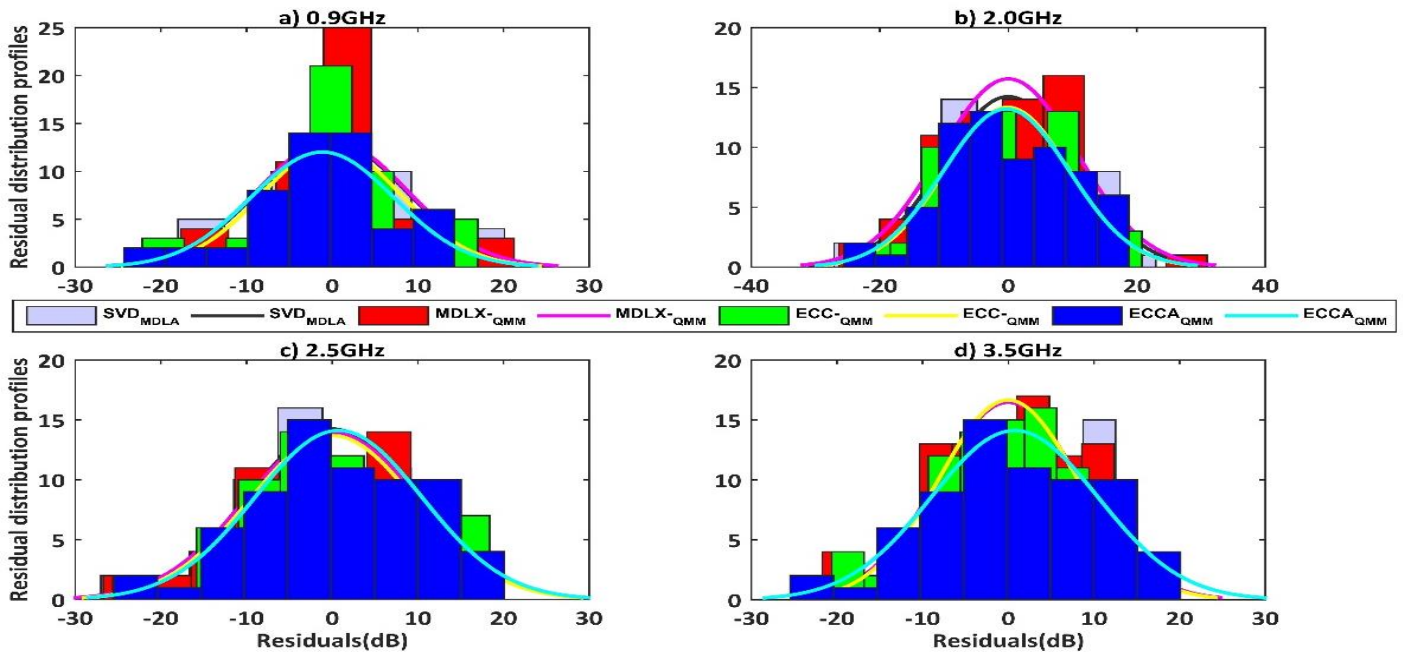
Figure 14: Histogram and normal density function plots for the residuals of pathloss profiles of Figure 13
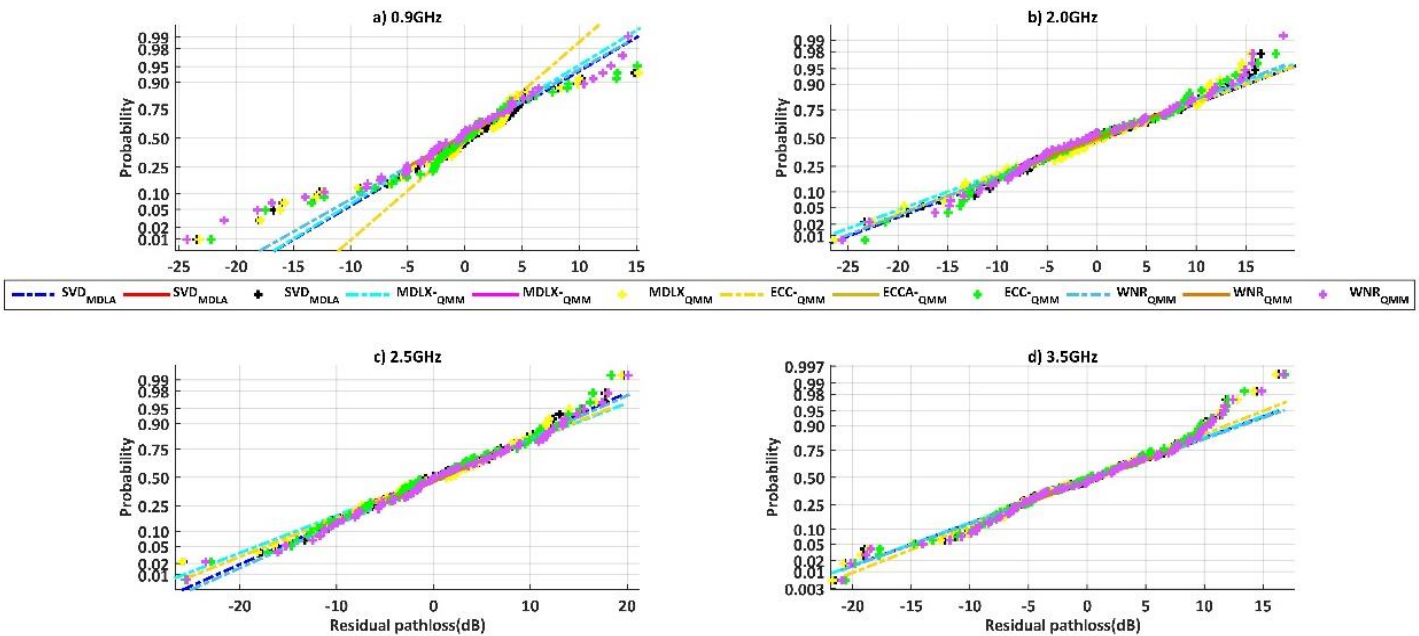

Figure 15: Normal probability curves corresponding to Figure 14

When compared with the corresponding metrics of Table 2, it is seen that all the alternative models have better RMSPE and MPE metrics than the base models from which they derived. Indeed, the improvement in MPE of the SVD calibration over those recorded by the coefficients of Table 2 of [10] is truly remarkable. These improvements are reflected in the pathloss profiles of Figure (13) as well as the histogram and normal probability plots of Figs. (14) and (15).

It is worth noting that in virtually all cases of the

alternative models, RMSPE metrics are about the same except for those for the alternative ECC33 models, which in general, are the best, but with correspondingly generally poorer MPE metrics.

When the same alternative models were calibrated with measurements of Figure (2b) of [10], results similar to those described for the Figure (2a) cases were obtained. In this case, the calibration coefficients emerged as shown in Table 11.

**Table 11:** Calibration coefficients for the alternative models calibrated with Fig (2b) ([10]) measurements

Frequency (GHz)	QMM Models ECC33 $(\alpha_1, \alpha_2, \ldots \alpha_5)$	WINNERII $(\alpha_1, \alpha_2, \alpha_3, \alpha_4)$	MODEL X $(\alpha_1, \alpha_2, \alpha_3)$	SVD MODEL X $(\alpha_1, \alpha_2, \alpha_3)$
0.9	140.1527 1.2400 3.4313 - 1.1795 727.0991	33.4173 1.9724 5.9726	33.5561 3.6850 2.4563	33.5417 3.6854 2.4670
2.0	-26.1012 0.0315 0.1882 1.1674 10.2215	42.7621 1.5681 7.8095	42.8194 2.9307 10.5625	42.7905 2.9313 10.5857
2.5	285.1581 -13.9642 46.3880 - 5.3848 76.8877	-76.8195 3.6952 13.3601	-82.9381 7.0482 95.9139	-76.9928 6.9149 91.1494
3.5	146.2949 2.8452 2.3526 - 2.3206 -90.3415	0.2384 1.9642 11.3583	0.2232 3.6734 55.9607	0.2268 3.6733 55.9579

Table 12: Performance metrics for the alternative models defined by the coefficients of Table 11

FREQ / MODEL	0.9GHz		2.0GHz		2.5GHz		3.5GHz	
	MPE	RMSPE	MPE	RMSPE	MPE	RMSPE	MPE	RMSPE
X_{SVD}	-0.0006	6.9341	0.0006	8.6148	0.0007	7.1023	-0.0000	7.4999
X_{QMM}	0.0002	6.9341	-0.0002	8.6148	0.0808	7.1049	-0.0001	7.4999
ECC_{QMM}	0.0308	6.9140	0.0043	8.5913	0.4688	6.5033	0.0190	7.2552
WIN_{QMM}	-0.0001	6.9341	-0.0031	8.6148	0.0029	7.1023	-0.0026	7.4999

Performance metrics for the alternative models are displayed in Table 12, and it is readily observed through a comparison of the MPE and RMSPE of Tables 4 and 12, that the general trend is similar to that earlier described for the models' calibration with measurements of Figure (2a).
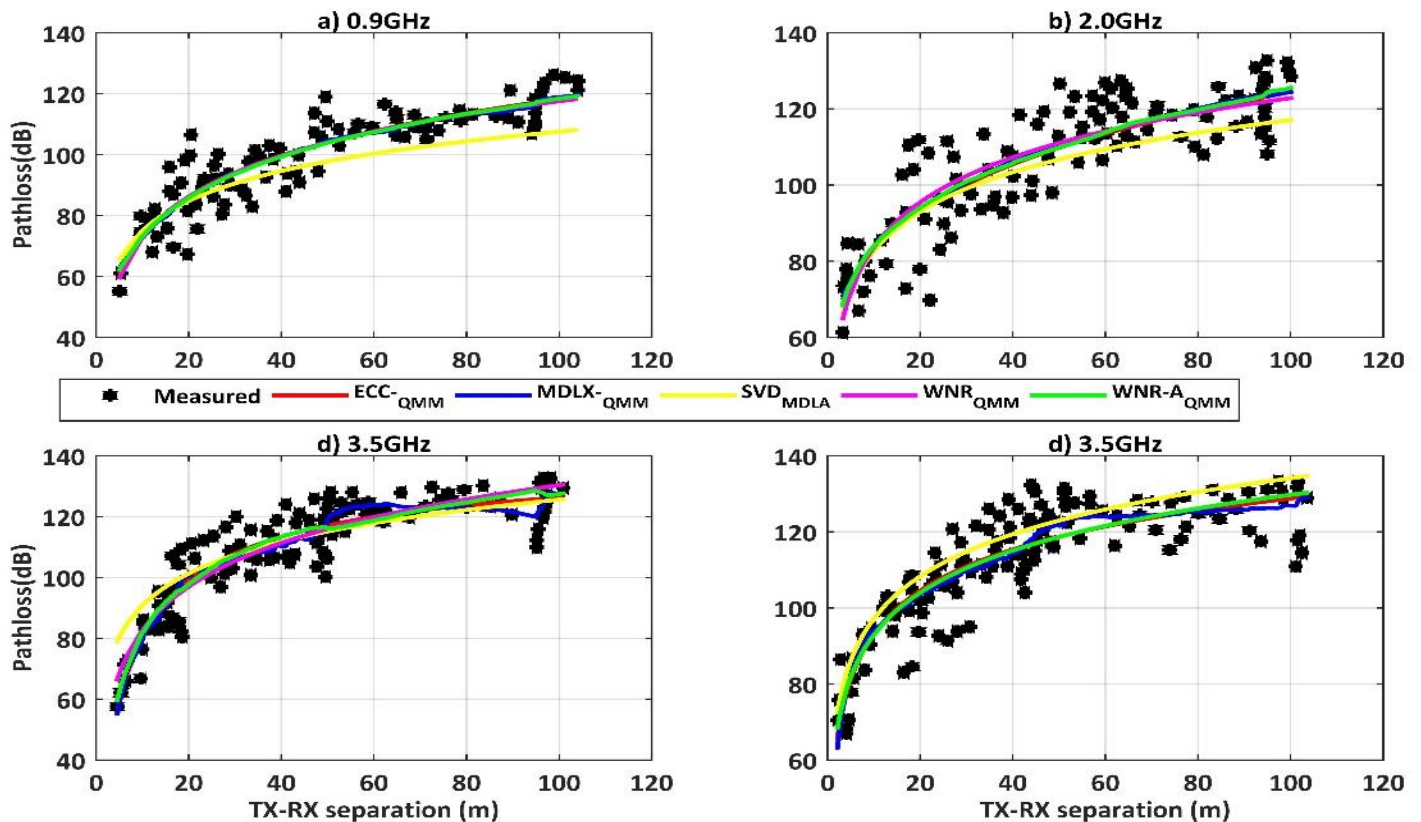
Figure 16: Comparison of pathloss prediction profiles for base and alternative models calibrated with Figure (2b) ([10]) measurements.
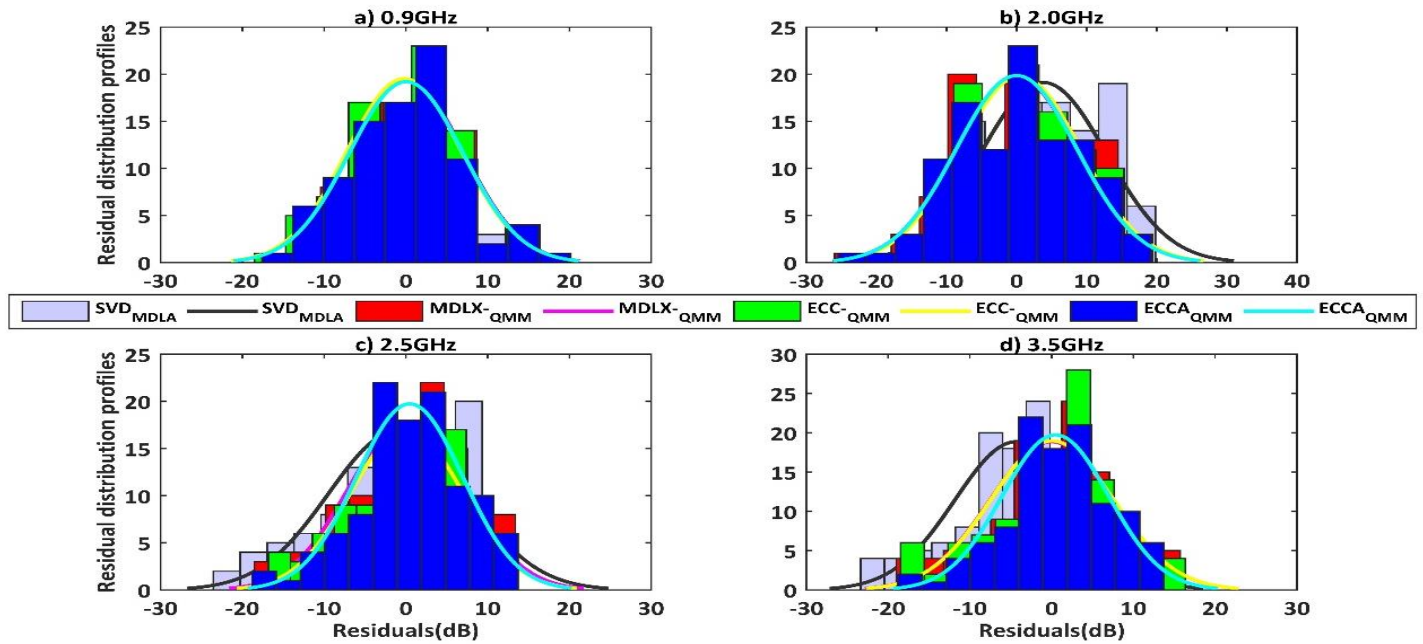
Figure 17: Histogram plots for the residuals due to the profiles of Figure (16)
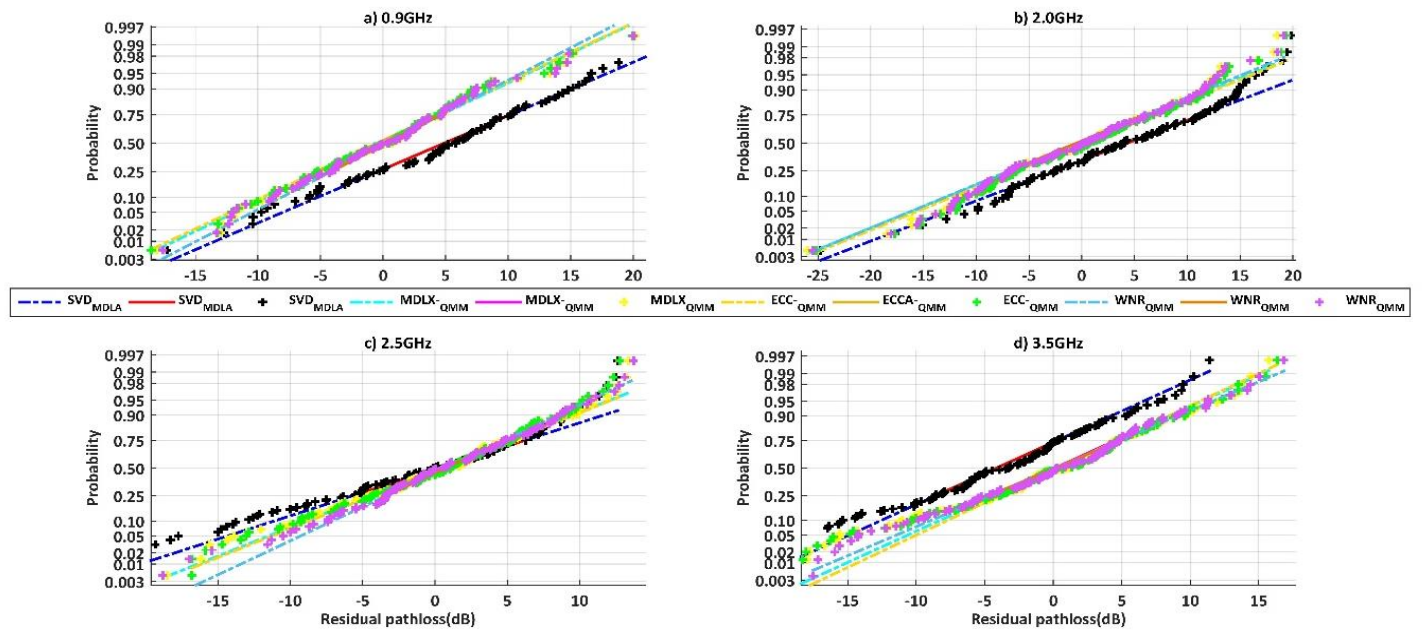

Figure 18: Normal probability plots for the residuals of Figure (17)

One noteworthy difference in this case is that RMSPE metrics are the same for models A and its alternative, model X.

The profiles of pathloss predicted by the base models and their corresponding alternatives reflect the differences and similarities just alluded to, as do the histogram and normal probability plots of Figs. (17) and (18).

3.2.2 Calibration with measurements of Figure 3(a) and 3(b) of [10]

Alternative base models calibrated with measurement data available from Figure (3a) and Figure (3b) of [10] are those defined by Eqn. (20), (21), and (22b) for 'Model Y', ECC33, and WINNERII (NLOS) cases, respectively. Model calibration coefficients due to calibration with Figure (3a) measurement data are as shown in Table 13.

Table 13: Model calibration coefficients for the alternative models calibrated with Fig (3a) ([10]) measurements

| Frequency (GHz)	ECC33 $(\alpha_1, \alpha_2, \ldots \alpha_5)$	QMM Models WINNERII $(\alpha_1, \alpha_2, \alpha_3, \alpha_4)$	MODEL Y $(\alpha_1, \alpha_2, \alpha_3, \alpha_4)$	SVD MODEL Y $(\alpha_1, \alpha_2, \alpha_3, \alpha_4)$
0.9	-63.6802 2.0510 -4.6068 1.4688 128.1705	19.2699 1.2442 -23.5729 1.2725	265.7984 1.3079 -99.7860 -4.1486	264.8864 1.3126 -99.3468 -4.1335
2.0	-79.7394 -2.9440 3.2499 2.1515 130.7895	30.8059 0.7623 -18.4795 7.5147	332.9813 -0.0460 -120.1142 -5.8019	331.9956 -0.0392 -119.6506 -5.7841
2.5	-208.7238 1.9297 -13.1051 4.8470 74.8624	85.2367 0.4360 -93.0314 41.6453	478.7392 -0.1968 -191.6983 -6.8199	474.6813 -0.1822 -189.7473 -6.7521
3.5	-145.7104 -2.8914 1.3073 3.3876 87.3625	32.3121 1.0283 -1.2066 0.6166	283.4954 0.9377 -97.2981 -5.1376	283.5972 0.9379 -97.3502 -5.1400

Table 14: Performance metrics for the alternative models defined by the coefficients of Table 13

FREQ / MODEL	0.9GHz MPE	RMSPE	2.0GHz MPE	RMSPE	2.5GHz MPE	RMSPE	3.5GHz MPE	RMSPE
Y	0.0001	4.6678	-0.0001	7.5664	0.0004	9.0715	0.0006	7.3036
Y$_{QMM}$	0.0000	4.6678	0.0002	7.5664	-0.0007	9.0715	-0.0001	7.3036
ECC$_{QMM}$	-0.0380	4.8560	0.0322	8.2013	-0.1332	9.0186	0.0121	7.6285
WIN$_{QMM}$	0.0014	4.9043	-0.0015	8.2411	-0.0015	9.2141	-0.0018	7.7283

According to the performance metrics of Table 14 compared with those of Table 6, the alternative model defined by the calibration coefficients of Table 13 gave significantly better prediction performances than the base models from which they derived.

A comparison of the metrics of Tables 6 and 14 readily reveals that RMSPE for model Y, improved between 6.2% (at 0.9GHz) and close to 62% (at 3.5GHz) over corresponding values for model B. The QMM calibration of the two models attracted relatively modest improvements (between 6% and 9%) for model Y over model B. It is interesting to observe that in the cases of the alternative ECC33 and WINNERII models, RMSPE remained about the same as for the corresponding base models.
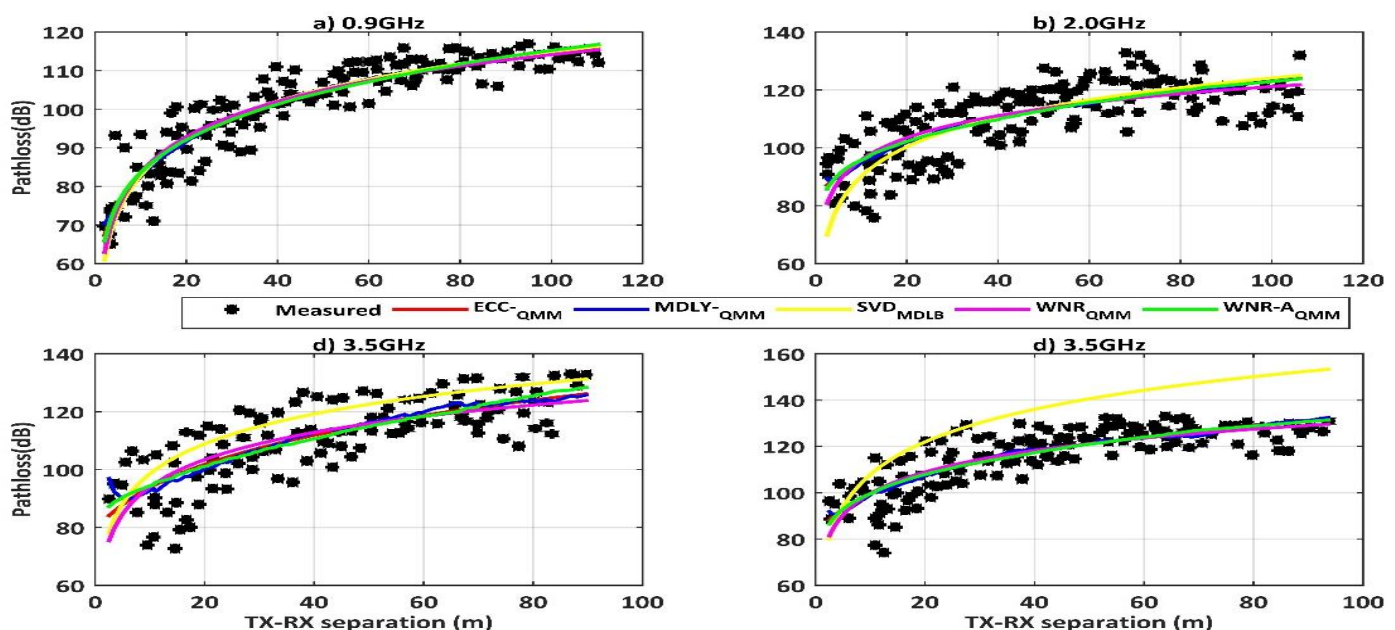
Figure 19: Comparison of pathloss predicted by base and alternative models calibrated with measurements of Fig 3(a) ([10])
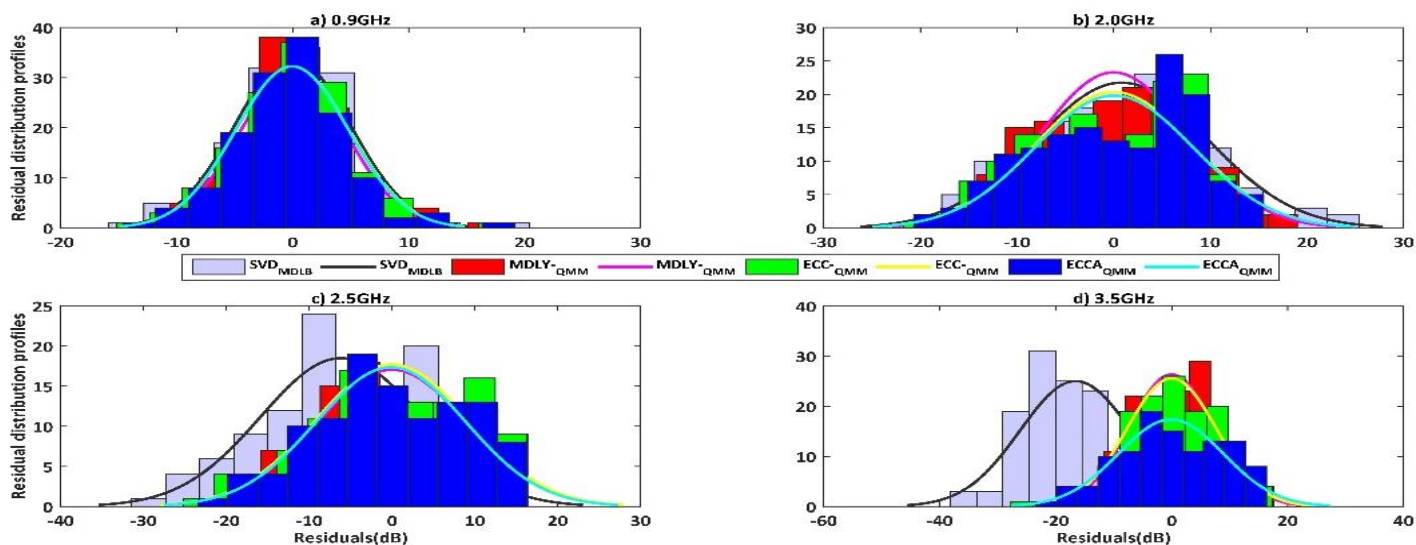
Figure 20: Histogram and density function plots for the residuals of the profiles of Figure (19)
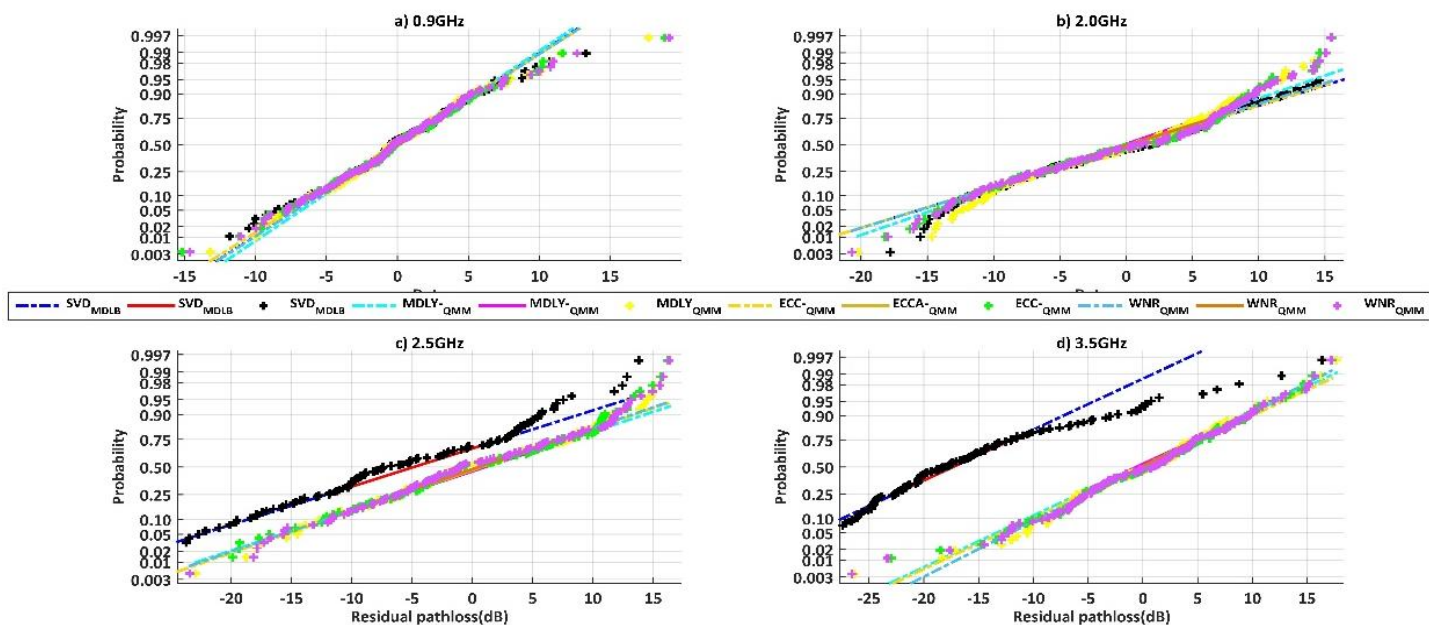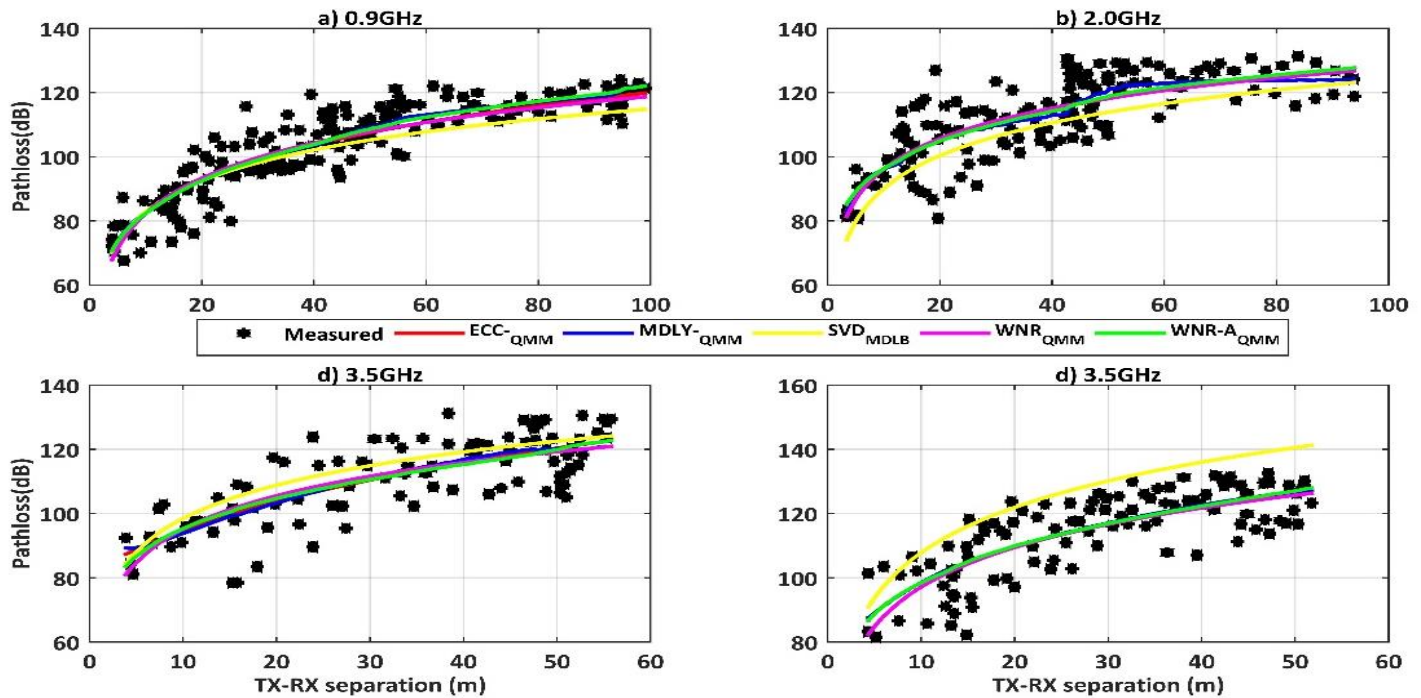

Figure 21: Normal probability plots for the residuals of Figure (19)

Table 15: Model calibration coefficients for the alternative models calibrated with Fig (3b) ([10]) measurements

Frequency (GHz)	QMM Models			SVD
	ECC33	WINNERII	MODEL Y	MODEL Y
	$(\alpha_1, \alpha_2, \ldots \alpha_5)$	$(\alpha_1, \alpha_2, \alpha_3, \alpha_4)$	$(\alpha_1, \alpha_2, \alpha_3, \alpha_4)$	$(\alpha_1, \alpha_2, \alpha_3, \alpha_4)$
0.9	-60.2819 4.3776 - 4.4181 -0.8073 888.4816	26.6602 1.3719 -0.5282 -1.8418	91.2207 2.3103 -16.5804 -1.4535	91.2683 2.3100 -16.6026 -1.4545
2.0	106.4024 -3.4930 13.3272 -1.8640 37.8967	26.3114 1.1006 0.1508 -0.1131	67.9812 2.0922 3.3618 -1.0386	68.0235 2.0915 3.3437 -1.0392
2.5	-59.2294 1.0640 - 6.5136 2.7097 26.1650	29.2339 1.3371 22.6619 4.7056	-111.1452 0.9629 94.4632 5.1760	-111.1378 0.9631 94.4587 5.1756
3.5	-27.1590 0.6898 - 1.1074 1.3364 -1.8379	25.6892 1.5410 -3.3084 -1.6843	386.0457 3.2535 - 154.2601 -12.1499	383.0595 3.2582 - 152.8365 -12.0550

Table 16: MPE and RMSPE metrics for the models defined by Table 15

FREQ /	0.9GHz		2.0GHz		2.5GHz		3.5GHz	
MODEL	MPE	RMSPE	MPE	RMSPE	MPE	RMSPE	MPE	RMSPE
Y_{SVD}	-0.0009	5.8650	0.0002	7.9124	0.0005	8.3235	0.0003	7.8655
Y_{QMM}	0.0003	5.8650	-0.0002	7.9124	0.0002	8.3235	0.0004	7.8655
ECC_{QMM}	-0.0431	5.9793	0.1289	7.8690	-0.0633	8.3182	-0.0108	8.0947
WIN_{QMM}	0.0043	5.9906	0.0020	7.9759	-0.0022	8.4512	0.0042	8.1007

Figure 22: Profiles of pathloss predicted by base alternative models calibrated with Figure (3b) ([10]) measurements

The much more pronounced differences in the profiles of Figure (19) at 2.5 GHz ad 3.5GHz are consistent with the metrics of Tables 6 and 14, and are reflected in the histogram and normal probability plots of Figs. (20) and (21).

Finally, the model calibration coefficients due to calibrations with measurement from Figure 3(b) of [10] are presented in Table 15.

For the models defined by these coefficients, pathloss prediction performance is described by the MPE and RMSPE metrics of Table 16. And as was the case with the corresponding metrics of Table 14, the RMSPE metrics for the SVD/QMM model Y represent improvements over the model B metrics; in this case, about 16% for each of the 0.9GHz, 2.0GHz, and 2.5GHz models, and close to 48% for the 3.5GHz model.

The calibrated alternative ECC33 and WINNERII models also recorded improved metrics over those for the calibrated nominal base models; the improvements ranged between about 1.5% at one extreme to about 4.56% at the other.

Improvements recorded by the corresponding MPE metrics for these calibrated alternative base models (and indeed, for the cases of other alternative models earlier discussed) are particularly remarkable, as can be seen from Table 16. The associated pathloss characteristics predicted by the calibrated alternative models are compared with those of their 'parent' base models by the profiles of Figure (22).

Figures (23) and (24) characterize the relative shadow fading properties predicted by these models for the measurement environment, in terms of histogram / normal density function and normal probability plots, respectively, due to the residuals due to the prediction by the models. It is noteworthy that for all the cases considered in this paper, the ECC33 model consistently recorded the best RMSPE metric, and although the model's corresponding MPE metrics compared favourably with those of the other calibrated models, those for the latter were better in all cases.
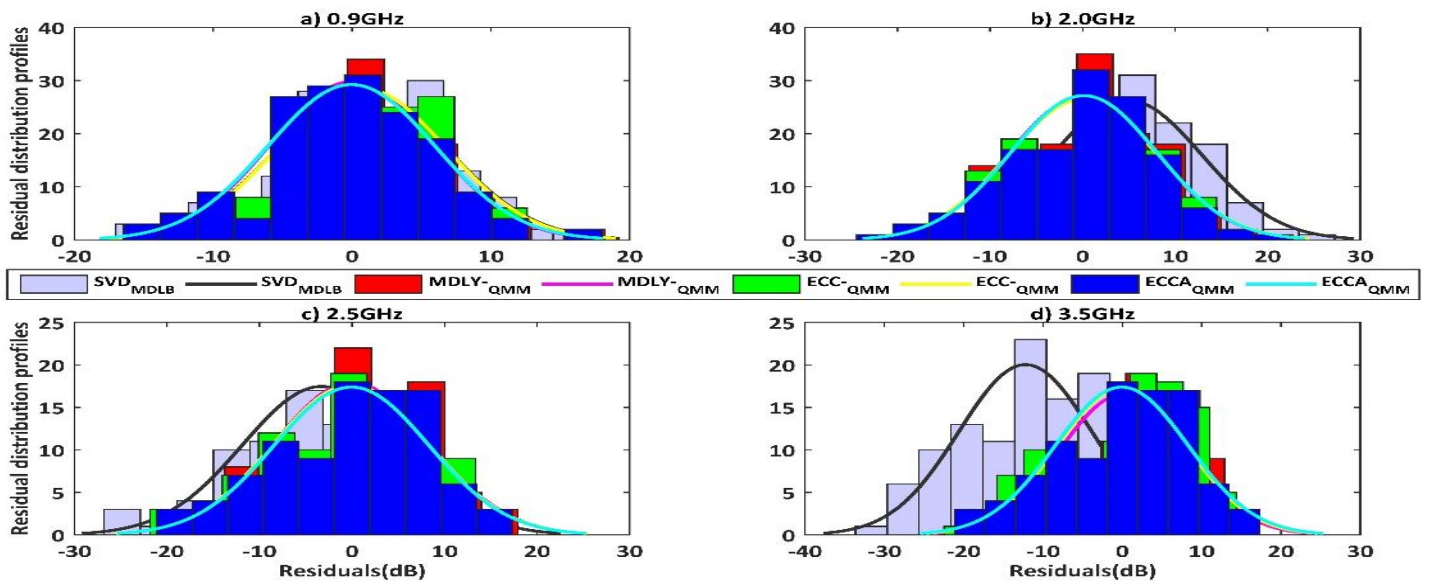
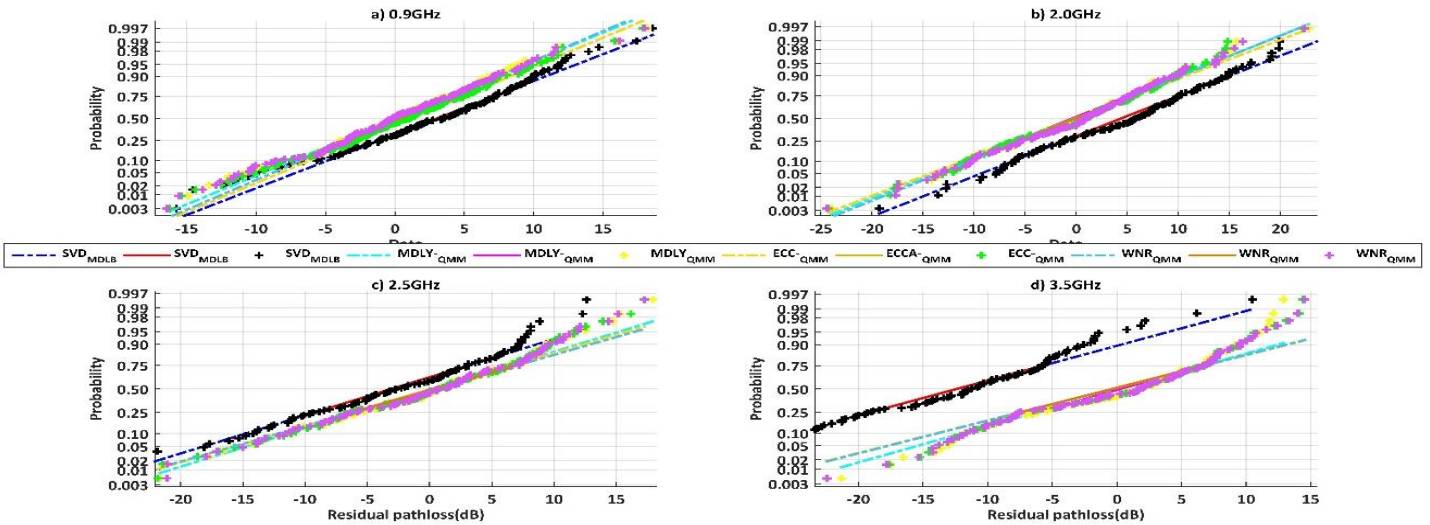**Figure 23:** Histogram/density function plots for the residuals of the pathloss profiles of Figure (22)

Figure 24: Normal probability plots corresponding to Figure (23*)*

4.0 CONCLUDING REMARKS

This paper has systematically and comprehensively investigated the equivalence of Singular Value Decomposition (SVD) and the Quasi-Moment-Method (QMM) as tools for the calibration of basic (nominal) radiowave propagation pathloss models. First, a performance comparison of QMM-calibrated ECC33 and WINNERII models on one hand and published (corresponding) SVD models on the other, suggested that the QMM-calibrated models have better prediction characteristics. However, after identifying some inconsistencies concerning the 'design' matrices and associated calibration coefficients in a recent publication, [10], this paper prescribed alternative base models, defined to eliminate the inconsistencies. Outcomes of the calibration of the alternative base models verified the paper's earlier

analytically established fact that the QMM and SVD algorithms represent equivalent alternative implementations of the same calibration scheme. Nonetheless, the FORTRAN (FORCE 2.0.9) implementation of the schemes indicated that whereas the QMM calibration of the alternative ECC33 and WINNERII models is computationally stable, corresponding SVD implementations produced what the computer referred to as 'badly-scaled' model calibration matrices. The implication of this observation is that unlike QMM, SVD becomes applicable only when collinearity is eliminated, and if the design matrix is consequently singular value decomposable.

A particularly interesting outcome of the investigations is indication by the computational results, that the basic ECC33 model (more popular with pathloss for outdoor environments), when subjected to QMM-

calibration, gives better RMSPE metrics than those due to the basic WINNERII models, which are specific to indoor-to-outdoor modelling.

It is also of interest to observe that the modelling of video quality loss estimation reported by Matos et al [16] utilized an empirical approach, whose features, as described by the publication's Eqn. (3) and (4), very clearly define an SVD algorithm. This suggests that the QMM/SVD solution developed here can find advantageous application in the empirical modelling of video quality loss. Another application possibility is prescribed by a recommendation due to Anamonye, Efenedo, and Okuma, [17], for the development of a readily adaptable model, capable of being easily calibrated with measurements taken in a significantly changing wireless communication environment.

REFERENCES

[1] Janaswamy, R. "An Indoor Pathloss Model at 60 GHz Based on Transport Theory", *Institute of Electrical and Electronics Engineers, Antennas and Wireless Propagation Letters*, 5, 2006, pp. 58-60. doi: https://10.1109/LAWP.2006.870361.

[2] Diago-Mosquera, M.E., Aragón-Zavala, A., and C. Vargas-Rosales. "The performance of in-building measurement-based path loss modelling using kriging", *Institution of Engineering and Technology, Microwaves Antennas & Propagation,* 15(12), 2021, pp. 1564-1576. doi: https://doi.org/10.1049/mia2.12163.

[3] Norberti, L., Nebuloni, R., and Magarini, M. "Characterization of the Indoor-to-Outdoor Wireless Channel in Air-to-Ground Communication Systems", 16th *International Conference on Wireless and Mobile Computing, Networking and Communications (WiMob)*, 2020, pp. 1-6. doi: https://10.1109/WiMob50308.2020.9253373.

[4] Okamoto, H., Kitao, K., and Ichitsubo, S. "Outdoor-to-Indoor Propagation Loss Prediction in 800-MHz to 8-GHz Band for an Urban Area", *Institute of Electrical and Electronics Engineers Transactions on Vehicular Technology*, 58(3), 2009, pp. 1059- 1067. doi: https://10.1109/TVT.2008.927996.

[5] Celik, S., Yoruk, Y. E., Bitirgan, M., Kurnaz, O., Basyigit, B., Helhel, S., and Izen S. "Indoor to outdoor propagation model improvement for GSM900/GSM1800/CDMA-2100", *2011 XXXth URSI General Assembly and Scientific Symposium*, 2011, pp. 1-4, doi: https://10.1109/URSIGASS.2011.6050535.

[6] Rodriguez, I., Nguyen, H. C., Kovács, I. Z., Sørensen, T. B., and Mogensen, P. "An Empirical Outdoor-to-Indoor Path Loss Model From Below 6 GHz to cm-Wave Frequency Bands", *Institute of Electrical and Electronics Engineers, Antennas and Wireless Propagation Letters*, 16, 2017, pp. 1329- 1332. doi: https://10.1109/LAWP.2016.2633787.

[7] Gimenez, J. J., Jansen, T., Rose, D., and Cardona, N. "Indoor-to-Outdoor Measurement Campaign for the Development of a Propagation Model for Femtocell Environment", *5th COST IC1004 Meeting*, Bristol, September, 2012. Downloaded from https://www.researchgate.net/publication/278410719

[8] Artemenko, O., Rubina, A., Nayak, A. H., Menezes, S. B., and Mitschele-Thiel, A, "Evaluation of different signal propagation models for a mixed indoor-outdoor scenario using empirical data", *EAI Endorsed Transaction on Mobile Communications and Applications*, 6(7), 2016. pp. 1-8. doi: https://10.4108/eai.20-6-2016.151519

[9] Valcarce, A. and Zhang, J. "Empirical Indoor-to-Outdoor Propagation Model for Residential Areas at 0.9–3.5 GHz", *IEEE Antennas and Wireless Propagation Letters,* 9, 2010, pp. 682-685. doi: https://10.1109/LAWP.2010.2058085.

[10] Allen, B., Mahato, S., Gao, Y., and Salous, S. "Indoor-to-outdoor empirical path loss modelling for femtocell networks at 0.9, 2, 2.5 and 3.5 GHz using singular value decomposition" *Institute of Electrical and Electronics Engineers, Microwaves Antennas and Propagation*, 11(9), 2017, pp. 1203- 1211. doi: https://doi.org/10.1049/iet-map.2016.0416.

[11] Adekola, A., Ayorinde, A., Okewole, F., and Mowete, Ike. "A Quasi-Moment-Method empirical modelling for pathloss prediction", *International Journal of Electronics Letters*, 2021. doi: https://10.1080/21681724.2021.1908607.

[12] Mandel. J. "Use of the Singular Value Decomposition in Regression Analysis", *The American Statistician*, 36(1), 1982, pp. 15-24. doi: https://10.1080/00031305.1982.10482771.

[13] Adelabu, M. A., Ayorinde, A., Muhammed, H. A., Okewole, F. O., and Mowete. I. "An evaluation of Quasi-Moment-Method Calibrated Pathloss Models for Benin City Nigeria", *Nigerian Journal of Technology,* 40(3), 2021, pp. 473-483. DOI: https://dx.doi.org/10.4314/njt.v40i3.13.

[14] Ayorinde, A., Muhammed, H., Okewole, F., and Mowete, I. 2021. "A Novel Propagation Pathloss Model Calibration Tool", *International Journal on Communications Antenna and Propagation (IRECAP),* 11(3), 2021, pp. 166-180. doi: https://doi.org/10.15866/irecap.v11i3.19796.

[15] Pimienta-del-Valle, D., Mendo, L., Riera, J. M., and Garcia-del-Pino, P. "Indoor LOS Propagation Measurements and Modeling at 26, 32, and 39 GHz Millimeter-Wave Frequency Bands", *Electronics,* 9(11), 2020, 1867. https://doi.org/10.3390/electronics9111867.

[16] Matos, E. M. C., Costa, T. A., Alcantara, M. C., Neto, B. S. L., Castro, F. S., Fatias, J. P. L., and Basros, F. J. B. "Video Quality Loss Model on Communication Networks: An Approach Based on Frame Loss', *Journal of Communication and Information Systems,* 37(1), 2022. pp. 42-46. doi: https://10.14209/jcis.2022.4.

[17] Anamonye, U. G., Efenedo, G. & Okuma, O. "Evaluation and Analysis of GSM Signals in Warri", *Nigerian Journal of Technology,* 38(3), 2016. pp. 568-578. doi: http://dx.doi.org/10.4313/njt.v35i1.15.